Effects of lower troposphere vertical mixing on simulated clouds and precipitation over the Amazon during the wet season

Xiao-Ming Hu[1], Yongjie Huang[1], Ming Xue[1], Elinor R Martin[1], Yang Hong[1], Mengye Chen[1], Hector Mayol Novoa[2], Renee A. McPherson[1], Andres Perez[2], Isaac Yanqui Morales[2], and Auria Julieta Flores Luna[2]

[1]University of Oklahoma
[2]Universidad Nacional de San Agustín de Arequipa

January 24, 2023

Abstract

Planetary boundary layer (PBL) schemes parameterize unresolved turbulent mixing within the PBL and free troposphere (FT). Previous studies reported that precipitation simulation over the Amazon in South America is quite sensitive to PBL schemes and the exact relationship between the turbulent mixing and precipitation processes is, however, not disentangled. In this study, regional climate simulations over the Amazon in January-February 2019 are examined at process level to understand the precipitation sensitivity to PBL scheme. The focus is on two PBL schemes, the Yonsei University (YSU) scheme, and the asymmetric convective model v2 (ACM2) scheme, which show the largest difference in the simulated precipitation. During daytime, while the FT clouds simulated by YSU dissipate, clouds simulated by ACM2 maintain because of enhanced moisture supply due to the enhanced vertical moisture relay transport process: 1) vertical mixing within PBL transports surface moisture to the PBL top, and 2) FT mixing feeds the moisture into the FT cloud deck. Due to the thick cloud deck over Amazon simulated by ACM2, surface radiative heating is reduced and consequently the convective available potential energy (CAPE) is reduced. As a result, precipitation is weaker from ACM2. Two key parameters dictating the vertical mixing are identified, p, an exponent determining boundary layer mixing and λ, a scale dictating FT mixing. Sensitivity simulations with altered p, λ, and other treatments within YSU and ACM2 confirm the precipitation sensitivity. The FT mixing in the presence of clouds appears most critical to explain the sensitivity between YSU and ACM2.

1 **Effects of lower troposphere vertical mixing on simulated clouds and precipitation over the**
2 **Amazon during the wet season**
3

4 Xiao-Ming Hu[1,2], Yongjie Huang[1], Ming Xue[1,2], Elinor Martin[2], Yang Hong[3], Mengye Chen[3],
5 Hector Mayol Novoa[4], Renee McPherson[5], Andres Perez[4], Isaac Yanqui Morales[4], Auria Julieta
6 Flores Luna[4]
7

8 [1] Center for Analysis and Prediction of Storms, University of Oklahoma, Norman, Oklahoma,
9 73072, USA
10 [2] School of Meteorology, University of Oklahoma, Norman, Oklahoma, 73072, USA
11 [3] School of Civil Engineering and Environmental Engineering, University of Oklahoma,
12 Norman, Oklahoma, 73072, USA
13 [4] Universidad Nacional de San Agustín de Arequipa, Arequipa, Perú
14 [5] Department of Geography and Environmental Sustainability, University of Oklahoma, Norman,
15 Oklahoma, 73072, USA
16

17 Submitted to

18 *Journal of Geophysical Research-Atmospheres*

19 on 1/19/2023 3:47 PM
20

21 Corresponding author address:
22 Drs. Xiao-Ming Hu (xhu@ou.edu), Ming Xue (mxue@ou.edu)
23 Hector Mayol Novoa (hnovoa@unsa.edu.pe),
24 Phone: (405) 325- 0402
25 Center for Analysis and Prediction of Storms, and School of Meteorology
26 University of Oklahoma
27 Norman, Oklahoma 73072, USA
28
29

30 **Key points:** (≤140 characters)
31

32   1. disentangle the turbulence/cloud/precipitation processes over Amazon and reveal root
33   causes for precipitation sensitivity to PBL schemes.

34   2. FT mixing becomes prominent in the presence of clouds, which in turn supports
35   maintenance of the FT clouds that would otherwise dissipate.

36   3. Stronger vertical moisture relay transport in ACM2 PBL scheme supports thicker FT
37   clouds, leading to reduced heating and precipitation.

38
39
40

1

41   **Abstract**

42   Planetary boundary layer (PBL) schemes parameterize unresolved turbulent mixing within

43   the PBL and free troposphere (FT). Previous studies reported that precipitation simulation over the

44   Amazon in South America is quite sensitive to PBL schemes and the exact relationship between

45   the turbulent mixing and precipitation processes is, however, not disentangled. In this study,

46   regional climate simulations over the Amazon in January-February 2019 are examined at process

47   level to understand the precipitation sensitivity to PBL scheme. The focus is on two PBL schemes,

48   the Yonsei University (YSU) scheme, and the asymmetric convective model v2 (ACM2) scheme,

49   which show the largest difference in the simulated precipitation. During daytime, while the FT

50   clouds simulated by YSU dissipate, clouds simulated by ACM2 maintain because of enhanced

51   moisture supply due to the enhanced vertical moisture relay transport process: 1) vertical mixing

52   within PBL transports surface moisture to the PBL top,   and 2) FT mixing feeds the moisture into

53   the FT cloud deck. Due to the thick cloud deck over Amazon simulated by ACM2, surface

54   radiative heating is reduced and consequently the convective available potential energy (CAPE) is

55   reduced. As a result, precipitation is weaker from ACM2. Two key parameters dictating the

56   vertical mixing are identified, p, an exponent determining boundary layer mixing and λ, a scale

57   dictating FT mixing. Sensitivity simulations with altered p, λ, and other treatments within YSU

58   and ACM2 confirm the precipitation sensitivity. The FT mixing in the presence of clouds appears

59   most critical to explain the sensitivity between YSU and ACM2.

60

61   **Plain Language Summary** (≤200 words)

62   Predictions of weather and climate in terms of clouds and precipitation over the Amazon

63   in South America are quite uncertain. This uncertainty has been largely attributed to errors in the

64   planetary boundary layer (PBL) scheme, which represents turbulent mixing.   A lack of

65   understanding of the relationship between turbulence, clouds, and precipitation processes prevents

66   us from improving PBL representation in models to achieve better weather and climate simulations.

67   This study disentangles the turbulence/clouds/precipitation relationship, and identifies the

68   root cause of model errors in PBL schemes using regional climate simulations over the Amazon.

69   Two PBL schemes, the Yonsei University (YSU) scheme, and the asymmetric convective model

70   v2 (ACM2) scheme, are examined, which show the largest difference in the simulated precipitation.

71   The main difference between the two PBL schemes is the dissipation (YSU) or maintenance

72   (ACM2) of clouds during daytime above the boundary layer, which modulates surface heating and

73   consequently precipitation. The maintenance of a thick cloud deck over the Amazon in ACM2, is

74   caused by enhanced vertical transport of moisture from the surface to above the boundary layer.

75   Such an improved understanding of the turbulence/clouds/precipitation relationship allow us to

76   propose potential solutions to improve PBL schemes in weather and climate models

77

78

81
82

1. Introduction

Climate change can cause shifted weather patterns, more extreme weather events, reduced water availability, change in agricultural patterns and increased exposure to disease (Langenbrunner et al., 2019; Prein et al., 2017; Vera et al., 2006) and other significant impacts on society. Accurate simulation of regional climate and the development of adaptation strategies and corresponding policies are critical. Global climate model (GCM) simulations are too coarse to resolve local forcing and local weather, and their precipitation simulation is generally poor. Cloud-resolving regional climate model (RCM) simulations have emerged in recent years for dynamically downscaling global climate simulations and climate change responses at spatial scales that are more useful for decision making (Huang et al., 2022; Liu et al., 2022; Prein et al., 2022; Prein et al., 2015; Prein et al., 2017; Sun et al., 2016). However, compared to mid-latitude regions, the performance of RCM simulations in reproducing precipitation over tropical regions, such as the Amazon in South America, is understudied (Chakraborty et al., 2020; Prein et al., 2022; Tai et al., 2021).

Noontime and afternoon mesoscale convective systems (MCSs) are the main source of precipitation over the Amazon and thus Amazonian precipitation has a single afternoon peak in diurnal cycle (Giangrande et al., 2017; Giangrande et al., 2020; Prein et al., 2022; Wu et al., 2021a). Moist advection from the Atlantic Ocean by northeasterly trade winds during the austral summer wet season (January - February) and zonal wind convergence are important for precipitation over the Amazon rainforest (Fu et al., 1999) and cloud and turbulence processes play critical roles in modulating precipitation in the region (Barber et al., 2022; Chakraborty et al., 2020; Chakraborty et al., 2018; Prein et al., 2022; Wright et al., 2017). The relationship between processes of clouds, turbulence, and precipitation in the region remains to be disentangled and their modelling uncertainties and sensitivities need to be understood to improve simulations (Giangrande et al., 2017; Giangrande et al., 2020; Prein et al., 2022).

Simulated precipitation over the Amazon is sensitive to the planetary boundary layer (PBL) scheme, but the root cause for such sensitivity and the cause-effect relationship remain to be disentangled (Prein et al., 2022). Within typical weather and climate models, PBL schemes parameterize unresolved turbulent mixing within the PBL and the free troposphere; the PBL schemes are therefore critical for reproducing the bulk boundary layer structures and profiles in the whole atmospheric column, as well as their subsequent effects on weather and climate

114   simulations. Many studies (Gunwani & Mohan, 2017; Hu et al., 2012; Hu et al., 2013a; Hu et al.,

115   2010a; Hu et al., 2019; Wang & Hu, 2021) have evaluated the performance of various modern

116   PBL schemes, with most of them focusing on continental cloud-free PBL. Compared to continental

117   clear PBL, much less is known about the performance of PBL schemes in presence of clouds

118   (Angevine et al., 2012; Huang et al., 2013; Supinie et al., 2022; Yang et al., 2019).

119   PBL schemes can be classified into local and nonlocal schemes. Local schemes estimate

120   the turbulent fluxes at each point in a model from the mean atmospheric variables and/or their

121   gradients at that point, whereas nonlocal schemes include turbulent fluxes based on the

122   atmospheric variables and their variations over a deeper layer covering multiple model levels

123   through the PBL (Cohen et al., 2015; Hu et al., 2010a). The assumption among local schemes that

124   fluxes depend solely on local values and local gradients of model state variables is least valid under

125   convective conditions when turbulent fluxes are dominated by large eddies that transport fluid over

126   longer distances (Hu et al., 2010a). Previous studies found that traditional local schemes (e.g.,

127   Mellor–Yamada–Janjić (MYJ) or quasi-normal scale elimination (QNSE)) predict daytime

128   continental boundary layers that are too cool and shallow; while schemes that include non-local

129   treatment, such as the Asymmetrical convective model, version 2 (ACM2, Pleim, 2007), the

130   Yonsei University (YSU, Hong et al., 2006) schemes and the more recently-updated local scheme

131   (e.g., Mellor–Yamada Nakanishi and Niino (MYNN, Nakanishi & Niino, 2006)) predict deeper

132   and warmer daytime continental boundary layers than MYJ and QNSE (Bright & Mullen, 2002;

133   Clark et al., 2015; Coniglio et al., 2013). Also, nonlocal PBL schemes can reproduce the slightly

134   stable upper convective boundary layer while local schemes often fail to do so (Hu et al., 2019;

135   Wang et al., 2016).

136   Recent PBL development has started to use the mass flux (MF) approach that has been

137   commonly used in cumulus parameterization schemes for large-eddy nonlocal mixing together with the

138   eddy-diffusivity (ED) closure parameterizing local mixing, such as the MYNN-EDMF scheme (Angevine

139   et al., 2010; Olson et al., 2019a; Olson et al., 2019b; Pergaud et al., 2009). Most previous PBL

140   modeling studies focus on treatments within the boundary layer while free-troposphere treatments

141   rarely receive much attention (Hu et al., 2012; Lu & Wang, 2019; Zhu et al., 2021; Zhu et al.,

142   2019), likely because that free-troposphere turbulence is weak under clear conditions and the

143   impact of its parameterization on weather and climate simulations is regarded as minor.

144   Huang et al. (2022) conducted nested-domain RCM simulations with grid spacings of 15

145   and 3 km over the Amazon with different physics schemes. It is found that the simulated

146   precipitation is most sensitive to PBL schemes with the YSU scheme significantly overpredicting

147   Amazonian precipitation and the ACM2 scheme predicting the weakest precipitation. Extending

148   the work of Huang et al. (2022), this study aims to understand the precipitation sensitivity over the

149   Amazon at a process level and identify the root cause for the different model behaviors, with

150   particular attention paid to the behaviors and effects of PBL schemes in cloudy environments, and

151   both inside and above the PBL. Effects of lower troposphere vertical mixing on simulated clouds

152   and precipitation over the Amazon will be elucidated.

153   The rest of this paper is organized as follows: In section 2, precipitation data, model

154   configurations, and numerical experiment design are described. In section 3, clouds/precipitation

155   sensitivity to PBL schemes is diagnosed using simulations with YSU and ACM2 and their variants

156   with altered turbulence treatments, followed by discussion of such sensitivity at a finer resolution.

157   Meanwhile the turbulence/cloud/precipitation processes over the Amazon are examined. Finally,

158   section 4 contains a summary and discussion of the main findings.

159

160   2. Precipitation data, model configuration and numerical experiment design

161   a) Precipitation data

162   Two gridded global precipitation datasets are used in this study to compare with

163   simulations, including (1) half-hourly Integrated Multi-satellitE Retrievals for GPM (IMERG) at

164   a horizontal resolution of $0.1° \times 0.1°$ (Huffman et al., 2019), and (2) half-hourly National Oceanic

165   and Atmospheric Administration (NOAA) Climate Prediction Center (CPC) MORPHing

166   Technique (CMORPH) global precipitation analyses at a horizontal resolution of ~8 km (Joyce et

167   al., 2004).

168

169   b) Model configurations

170   Huang et al. (2022) used the Weather Research and Forecasting (WRF) model Version

171   4.2.1 (Skamarock & Klemp, 2008; Skamarock et al., 2021) to perform historical simulations over

172   South America during January-February 2019 in preparation for future regional climate dynamic

173   downscaling. The simulations used hourly European Centre for Medium-Range Weather Forecasts

174   Reanalysis v5 (ERA5, Hersbach et al., 2020) for initial and boundary conditions. Two one-way

175 nested domains with 15- and 3-km horizontal grid spacings cover the entire South America and
176 the Peruvian central Andes region, respectively (see Fig. 1a for domain coverage). Both domains
177 use 61 stretched vertical levels topped at 20 hPa. Following previous dynamic downscaling
178 practices (Hu et al., 2018; Miguez-Macho et al., 2004, 2005; Wang & Kotamarthi, 2013), spectral
179 nudging technique is applied to the outer 15-km domain to maintain large-scale circulations at a
180 1500 km scale, while allowing WRF to evolve smaller-scale dynamics and physics. Twelve
181 sensitivity experiments were conducted by Huang et al. (2022) with varied PBL, microphysics
182 schemes, and land surface models while other physics parameterizations were kept the same
183 among the sensitivity experiments, including revised MM5 Monin-Obukhov surface layer scheme
184 (Jiménez et al., 2012), and the Rapid Radiative Transfer Model for GCMs (RRTMG) longwave
185 and shortwave radiation scheme (Iacono et al., 2008). The Tiedtke cumulus parameterization
186 scheme (Tiedtke, 1989) is used on the 15-km outer domain but not on the 3-km inner domain.

187 These WRF downscaling simulations are found to be most sensitive to PBL schemes with
188 the YSU scheme significantly overpredicting Amazonian precipitation, the ACM2 scheme
189 predicting the weakest precipitation, and the MYNN-EDMF prediction being in the middle. Such
190 relative differences are maintained with altered microphysics schemes and land surface models
191 (LSMs). Simulations with the Thompson microphysics scheme (Thompson et al., 2008), and the
192 Noah LSM (Chen & Zhang, 2009) are chosen to investigate PBL sensitivities in this study.
193 Diagnosing the root cause for the differences between the YSU and ACM2 PBL schemes and
194 disentangle the impact of PBL schemes on precipitation are the foci of this study. Since simulated
195 precipitation is quite sensitive to some other parameterization, such as cumulus schemes (Hu et al.,
196 2018), and there are large uncertainties among different precipitation data (Chen et al., 2022),
197 recommending an optimal PBL scheme in terms of reproducing precipitation is beyond the scope
198 of this study, which may require more advanced profile measurements (e.g., cloud water profile)
199 and more accurate precipitation data to justify as will be seen in our later analyses.

200

201 c) Sensitivity simulations with altered treatments in ACM2 and YSU

202 In addition to the simulations conducted by Huang et al. (2022), eight more sensitivity
203 simulations (summarized in Table 1) are run to help identify the root cause of the differences
204 between ACM2 and YSU, and resolution dependence of the differences, as well as to examine
205 impact of turbulent processes on cloud and precipitation processes. ACM2 and YSU differ in their

206   treatments in both PBL and free troposphere. Sensitivity simulations adjusting either PBL or free-

207   troposphere mixing treatments or both are conducted.

208   In the PBL, while a counter-gradient term is added to the eddy diffusion equation to handle

209   nonlocal mixing in YSU, ACM2 explicitly simulates the transilient nonlocal mass flux. For the

210   local mixing in the PBL, both ACM2 and YSU use a polynomial function/profile (so called K-

211   profile, Noh et al., 2003) to define the vertical mixing coefficient K_z as:

$$K_z = k \frac{u_*}{\varnothing} z (1 - \frac{z}{h})^p \qquad (1)$$

213   where k is the von Karman constant, ϕ is the similarity profile function, z is the height above ground

214   level, and h is the PBL height. Thus, ACM2 and YSU are also categorized into the K-profile PBL

215   schemes (Hu et al., 2019). In YSU and ACM2, the value of the exponent p in (1) is 2, but it may

216   vary from 0.5 to 3 depending on flow conditions, with a larger/smaller p yielding smaller/larger

217   K_z (Hu et al., 2018; Hu et al., 2010b; Nielsen-Gammon et al., 2010; Troen & Mahrt, 1986). While

218   a similar local mixing treatment is adopted in ACM2 and YSU, there are many differences in their

219   parameter values, profile functions, methods to diagnose PBL height, etc. ACM2 generally

220   simulates stronger vertical mixing in the PBL and higher PBL height under clear conditions (Hu

221   et al., 2010a). Since p effectively dictates the vertical mixing within the PBL, p is varied in

222   sensitivity simulations to understand model differences and physics processes including turbulence,

223   clouds, and precipitation.

224   In the free troposphere, both YSU and ACM2 compute the K_z as a function of mixing

225   length l, vertical wind shear S, and the stability function $f(Ri)$:

$$K_z = l^2 S f(Ri) , \qquad (2)$$

227   in which

$$\frac{1}{l} = \frac{1}{kz} + \frac{1}{\lambda} , \qquad (3)$$

229   where Ri is the Richardson number, and λ is the asymptotic length scale. Such first-order

230   parameterizations of turbulent vertical mixing are widely used in operational numerical weather

231   prediction (NWP) and climate models (Beare et al., 2006; Cuxart et al., 2006). ACM2 and YSU

232   differ in their parameter values, Ri calculation within clouds, and stability functions. Both ACM2

233   and YSU use moist-air Ri calculation adapted from Durran and Klemp (1982), but YSU requires

234   two layers of clouds to activate the moist-air Ri calculation between the two layers while ACM2

235   only requires one layer, in addition to other differences in parameters. Much of the improvement

236   to such parameterizations (Eqs. 2-3) in NWP and climate models involved adjusting the stability

237   functions (for example short vs. long-tailed functions) and λ (Cuxart et al., 2006). λ is adjustable

238   and varies between 30 and 250 m in numerical models (Cuxart et al., 2006; Liu & Carroll, 1996;

239   Nielsen-Gammon et al., 2010). λ is set to 30 m in the YSU scheme and to 80 m in the ACM2

240   scheme.   Sensitivity simulations are conducted in this study by replacing the whole free-

241   troposphere treatments or only altering the value of λ.

242   The sensitivity simulations are conducted with the outer 15 km domain because the

243   difference between inner-domain outputs from our nested-domain runs with different

244   configurations are rooted from the different simulations in the outer 15km domain, as we will see

245   in our analysis.   Thus, the conclusions from these sensitivity simulations have implications for

246   regional and global models that run at convection-parameterized resolutions.   In addition, four

247   sensitivity simulations with a single domain covering the majority of the Amazon with a 3 km grid

248   spacing are also conducted to examine the applicability of conclusions obtained at 15 km grid

249   spacing to convection-allowing simulations.

250

251   **3. Results**

252   a)   Cause of precipitation differences simulated with different PBL schemes

253   As stated earlier, WRF simulations over South America during January-February 2019 are

254   conducted with 12 different physics schemes, including PBL, microphysics schemes and land

255   surface models (Huang et al., 2022). The simulated precipitation is most sensitive to PBL schemes

256   (Huang et al., 2022) with the YSU scheme predicting the strongest daily precipitation rate while

257   the ACM2 scheme predicting the weakest precipitation over the Amazon during the summer wet

258   season (Fig. 1). The relative strength of simulated precipitation between ACM2 and YSU remains

259   across different resolutions, including the convection-parameterized (15 km grid spacing) and

260   convection-permitting (3 km grid spacing) resolutions.   The precipitation rate increases with

261   increased resolution. The YSU runs at 3 km grid spacing (including the nested run focusing on

262   Peru and the single-domain run focusing more on the Amazon) significantly overestimate daily

263   precipitation rate (Figs. 1c-f). The South America Affinity Group (SAAG) led by National Center

264   for Atmospheric Research (NCAR) also reported that a WRF simulation using the YSU scheme at

265   a grid spacing of 4 km over South America overestimated precipitation over the Amazon (Liu et

266   al., 2022).

267   Precipitation over the Amazon is dominated by mid-day and afternoon MCSs (Giangrande

268   et al., 2017; Giangrande et al., 2020; Prein et al., 2022; Wu et al., 2021a). Thus, we will focus on

269   the precipitation and related processes during daytime. During mid-day hours, YSU simulates

270   stronger hourly precipitation rates than ACM2 and overestimates precipitation at both resolutions

271   and over different domains (Fig. 2).

272   Causative factors for the different precipitation simulated by ACM2 and YSU over the

273   Amazon are herein investigated. The impact of different PBL schemes on NWP and climate

274   simulations is more straightforward under clear conditions while their impacts on precipitation is

275   less clear. Often the impact of PBL schemes on precipitation is not conclusive because the

276   schemes produce different (stronger or weaker) precipitation in different cases (Bright & Mullen,

277   2002; Cohen et al., 2015; Jankov et al., 2005; Jankov et al., 2007; Li & Pu, 2008; Supinie et al.,

278   2022; Wu et al., 2021b; Zhang et al., 2013). Under clear conditions, ACM2 simulates stronger

279   boundary layer vertical mixing and deeper PBL than YSU due to different treatments for nonlocal

280   fluxes and different parameters/functions in the K-profile local mixing (Hu et al., 2010a; Nielsen-

281   Gammon et al., 2010; Shin & Hong, 2011; Xie et al., 2012). How such differences translate to

282   significantly different precipitation with the two schemes is the main question to be answered in

283   this study.

284   Surface temperature shows distinct differences over the Amazon with the ACM2

285   simulating lower continental temperatures than YSU by 0.5-0.8 $^{\circ}$C over the simulation domains

286   around noon (Fig. 3), which likely leads to less surface energy to feed MCSs. The lower

287   temperature simulated by ACM2 covers the main precipitation region over the Amazon (Fig. 3g)

288   and can likely explain the precipitation difference. However, such temperature differences cannot

289   be explained by the direct impact of PBL mixing. Prior work has shown that during daytime,

290   ACM2 simulates stronger mixing in the PBL and stronger PBL-free troposphere exchange

291   generally warming up the PBL due to entrainment of free troposphere air with higher potential

292   temperature (Hu et al., 2010a; Shin & Hong, 2011). Thus, the direct impact of ACM2 PBL mixing

293 should lead to higher surface temperature, rather than the lower temperature obtained in the regions
294 of precipitation.

295   Rather, the temperature difference between ACM2 and YSU simulations is more directly
296 related to the difference in surface downward shortwave radiation. ACM2 simulates less
297 shortwave radiation at the surface over the Amazon region (Fig. 4g), where cloud coverage is
298 significant (Fig. 4j). At 17 UTC (12-14 LST across south America), the average surface shortwave
299 radiation simulated by ACM2 is lower by ~70 W m^{-2} than the YSU runs. Thus, the lower
300 temperature simulated by ACM2 should be due to indirect effects of vertical mixing via
301 interactions with clouds and radiation.

302   Significant cloud coverage over the Amazon (Kay et al., 2016; Kay et al., 2012) is a
303 characteristic distinguishing this study from most other studies of PBL schemes. Over the
304 Amazonian region, ACM2 simulates a thicker cloud deck (Fig. 5,6), which reduces downward
305 shortwave radiation (Fig. 7), consequently leading to a lower surface temperature. As a result, the
306 surface-based convective available potential energy (CAPE) is lower in the ACM2 simulations
307 (Fig. 8), which would lead to weaker daytime precipitation. The significant difference between
308 YSU and ACM2 is mostly confined over the cloud region (Fig. 4 & 7), which further confirms
309 that indirect effects of vertical mixing over the Amazon via interactions with clouds dominates its
310 direct effects.

311   The cloud deck over the Amazon therefore appears to be a critical link to disentangle the
312 impact of PBL schemes on simulated precipitation. During daytime, while the clouds simulated
313 with the YSU scheme dissipate gradually from the early morning maxima, clouds simulated with
314 the ACM2 scheme are still sustained through the day (see cloud cross-sections at 11 - 21 UTC in
315 Fig. 5). Daytime cloud thinning is likely due to solar heating under condition of lack of water
316 vapor supply available for condensation (Adebiyi et al., 2020; Burleyson & Yuter, 2015; Painemal
317 et al., 2015; Zhang et al., 2010). The thicker cloud deck simulated by ACM2 appears to be due to
318 enhanced supply of boundary layer moisture to the layers above (thus less boundary layer moisture
319 by 0.6 g kg^{-1} and more free troposphere moisture by 0.2 g kg^{-1} compared to the YSU run, Fig. 9b),
320 through enhanced boundary layer vertical mixing (Hu et al., 2010a; Shin & Hong, 2011).

321   In the nested-domain simulations, surface temperature simulated by ACM2 is lower than
322 YSU in both 15 and 3 km domains (Fig. 3) and the resulting lower precipitation occurs in both
323 domains. The root cause of lower surface temperatures from ACM2 in the nested 3 km domain is

324   less clear due to the possible effect of 15 km simulations (such as advection) through its lateral

325   boundaries. Thus, the main discussions below (in section b) will focus on further investigation of

326   PBL-clouds-precipitation relationship in the outer 15 km domain with additional simulations with

327   altered treatments, while their relationship at the convection-permitting resolution will be

328   examined with additional single-domain simulations with a 3 km grid spacing (in section c).

329

330   b) Impact of different turbulence treatments on clouds and precipitation

331   Lower troposphere turbulence plays important roles in cloud production and maintenance

332   (Lilly, 1968). This section discusses results of sensitivity simulations adjusting turbulence

333   treatments in YSU and ACM2. Since under clear conditions, ACM2 has stronger daytime

334   boundary layer mixing than YSU (Hu et al., 2010a; Shin & Hong, 2011), vertical mixing in the

335   YSU PBL scheme is first enhanced to see if the simulated clouds and precipitation would become

336   closer to those simulated by ACM2. The exponent p in the K-profile in YSU (default value is 2)

337   is reduced to 0.5 in experiment YSUp.5 to enhance daytime boundary layer mixing, as indicated by

338   the K_z profiles in Fig. 9d. With $p=0.5$, YSUp.5 simulates higher PBL top height (Fig. 9d). As a

339   result, more near-surface moisture is transported to the top of the elevated PBL, where a thicker

340   cloud layer near the PBL top forms (Fig. 6c & Fig. 9c). Note that while the nonlocal mixing is

341   proportional to K_z in YSU, transilient nonlocal fluxes are explicitly simulated by ACM2, which is

342   not shown in Fig. 9. Thus K_z profiles in Fig. 9d are more indicative of total mixing in the boundary

343   layer for YSU, but less so for ACM2. In the free troposphere where there are no nonlocal mixing

344   treatments for either scheme, thus K_z profiles are indicative of free-troposphere mixing for both.

345   As the PBL grows in the daytime, the PBL top clouds simulated by both YSU and ACM2

346   keep elevating (Fig. 5). A more prominent/distinct PBL top cloud layer is simulated by YSU (Fig.

347   5c,e, PBL top is marked by black dash lines) while the PBL top clouds simulated by ACM2 are

348   indistinctive from the free-troposphere clouds (Fig. 5d,f). Existence of a PBL top cloud layer over

349   the Amazon was previously illustrated by cloud frequency data observed during the GoAmazon

350   2014/5 field experiments (Giangrande et al., 2017; Giangrande et al., 2020). However, that dataset

351   only provides cloud frequency, not cloud amount. To quantitatively verify the simulated PBL top

352   cloud layer, more advanced cloud dataset is needed.

353   The thickened PBL top clouds simulated by YSU with $p=0.5$ weakens surface shortwave

354   radiation (Fig. 7) and consequently lowers surface temperature and CAPE (Fig. 8), thus reduces

12

355 precipitation (Fig. 10). Such a precipitation sensitivity to boundary layer mixing over the Amazon

356 is consistent with that reported over the eastern United States (Hu et al., 2018). However, YSU

357 with $p=0.5$ does not reduce precipitation to the level simulated by ACM2 (Fig. 10). In comparison,

358 ACM2 simulates a more prominent cloud layer at a higher elevation (~4-5 km above ground) while

359 the clouds simulated by YSU at this altitude (with both default p value and $p=0.5$) weaken in time

360 during the day (Fig. 5). Thus, boundary layer mixing alone cannot completely explain the different

361 impacts of ACM2 and YSU on clouds.

362　　　In addition to the different treatments within the boundary layer, ACM2 and YSU also

363 differ in their treatments in the free troposphere. A YSU sensitivity simulation using ACM2's

364 free-troposphere mixing treatment (named YSUuseACM2free) is conducted to examine the impact

365 of free troposphere mixing. YSUuseACM2free simulates a stronger vertical mixing up to 7-8 km

366 above the ground, particularly in presence of clouds, similar to the ACM2 simulation (Fig. 9d).

367 Further up, the sensitivity of vertical mixing is small and K_z is simulated to be less than 0.1 $m^2\,s^{-1}$

368 by all schemes. Thus, our analysis focuses on the lower free troposphere. As a result of stronger

369 mixing in the lower free troposphere, a thicker cloud deck at 4-5 km above ground (Fig. 6d), similar

370 to ACM2 (Fig. 6b), develops in the simulation, likely due to stronger moisture supply from the

371 PBL top. Consequently, surface temperature is reduced due to cloud shield, and the precipitation

372 is reduced, to be closer to that of ACM2 than YSUp. 5 (Fig. 10). Combining both $p=0.5$ and

373 ACM2's free-troposphere mixing, YSUp. 5useACM2free simulates a similar, but slightly thicker

374 cloud deck (Fig. 6e) and slightly weaker precipitation than YSUuseACM2free (Fig. 10). These

375 experiments illustrate that free-troposphere mixing is the most critical difference between YSU

376 and ACM2 in terms of simulating clouds and precipitation, while the mixing in the PBL plays a

377 secondary role.

378　　　For free troposphere vertical mixing, ACM2 and YSU differ in their parameters, moist-air

379 Ri calculation, and the stability functions. Previous studies identified λ as a critical parameter for

380 free-troposphere mixing (Cuxart et al., 2006; Hu et al., 2012; Nielsen-Gammon et al., 2010), and

381 here its impact is further examined. An ACM2 sensitivity simulation with $\lambda=30$ (named

382 ACM2λ30) is conducted to verify its impact on clouds/precipitation. Comparing to default ACM2

383 with $\lambda=80$, ACM2λ30 simulates a much weaker mixing in the free troposphere (Fig. 9d), and

384 consequently a much thinner cloud deck at 4-5 km above ground and meanwhile the PBL top

385 clouds appear thicker (Fig. 6f), likely due to weaker vertical transport of moisture from the PBL

386   top to higher levels. The net result is that the surface radiation is enhanced (Fig. 7f), temperature

387   is higher, and more precipitation is produced (Fig. 10f). The precipitation simulated by

388   ACM2λ30 is not as strong as that simulated by YSU because of other differences in free-

389   troposphere and PBL mixing treatments.

390   All the above results together suggest a prominent *PBL-free-troposphere moisture relay*

391   *transport process*: Step 1, boundary layer mixing transports moisture to the PBL top where clouds

392   form; step 2, free-troposphere mixing transports the moisture further to higher levels ($\sim$ 4-5 km)

393   to sustain a thick cloud deck at that altitude and reduce the boundary layer top clouds

394   somewhat. *ACM2 simulates a strong PBL-free-troposphere moisture relay transport process.*

395   Comparing to YSU, ACM2 simulates less PBL moisture (by 0.5 g kg^{-1}) and more free troposphere

396   moisture (by 0.2 g kg^{-1} at 3-6.5 km above ground, Fig. 9b) in monthly average. Consequently, the

397   free-troposphere cloud layer is better maintained during daytime. In contrast, the moisture relay

398   transport process simulated by YSU is weaker and the clouds at $\sim$ 4-5 km dissipate quicker during

399   daytime, leading to less cloud coverage, more CAPE and precipitation. Modified YSU with

400   enhanced PBL and free-troposphere mixing (YSUp.5useACM2free) produces similar moisture

401   transport as ACM2 (Fig. 9b,d) hence reduced precipitation. These results suggest that free-

402   troposphere mixing may become prominent in the presence of clouds (which otherwise would be

403   weak as generally regarded) and become an important step in the relay transport process. To verify

404   the strength of such relay transport process, more advanced observations, such as long-term

405   vertical profiles of cloud mixing ratios, are warranted. Our results also suggest that to correctly

406   simulate clouds/precipitation in environments similar to those of the Amazon, the ability of models

407   in reproducing such moisture relay transport processes needs to be carefully assessed.

408

409   *c)* Sensitivity of clouds and precipitation to different turbulence treatments at a convection-

410   allowing resolution

411

412   The sensitivity of simulated clouds and precipitation to boundary layer and free-

413   atmosphere vertical mixing discussed above is mainly based on simulations at 15 km grid spacing

414   where cumulus parameterization is employed. Thus, the conclusions are directly applicable to

415   global and regional weather and climate simulations/predictions at convection-parameterized

416   resolutions. Whether these conclusions are still valid at convection-permitting resolutions requires

417   additional examination. To avoid the possible effects of the driving 15 km grid on the nested 3

418 km grid, single-domain sensitivity simulations are conducted that cover a majority of the Amazon
419 with a 3 km grid spacing that use ERA5 data directly as lateral boundary conditions. These
420 simulations include 3kmYSU , 3kmYSUp.5 , 3kmYSUp.5useACM2free , and 3kmACM2 (as
421 summarized in Table 1). Even though simulated precipitation rate is generally higher at the 3 km
422 grid spacing than at 15 km grid spacing, the same turbulent mixing → clouds → precipitation
423 impact/sensitivity holds in these convection-permitting simulations (Fig. 11, 12). That is, 1) YSU
424 simulates stronger daytime precipitation rate than ACM2 (by 60% at noon time, 16 vs. 10 mm day$^-$
425 ^{1}, Fig. 12a,b); 2) Stronger boundary layer mixing simulated by YSU with p=0.5 leads to more PBL
426 top clouds (Fig. 11c), which block more shortwave radiation and reduce daytime surface
427 temperature and consequently precipitation (with 13 mm day^{-1} at noon, Fig. 12c); 3) Using the
428 free-troposphere mixing treatment of ACM2 in YSU simulates a more prominent cloud layer at 4-
429 5 km above ground (Fig. 11d) which more effectively blocks shortwave radiation and reduces
430 precipitation (with 11 mm day^{-1} at noon, Fig. 12d) that is closer to the precipitation rate of ACM2
431 (Fig. 12b).
432

433 **4. Conclusions and discussion**
434   Previous studies by others and a recent study of ours found that precipitation simulations
435 over the Amazon in South America are very sensitive to the PBL scheme used. The exact
436 relationship between the turbulent mixing and precipitation processes in that humid region is,
437 however, not clear. In this study, two-month-long simulations over South America in January-
438 February 2019 are examined to understand the precipitation sensitivity to treatments of turbulent
439 mixing in both the PBL and free troposphere within PBL schemes. Two PBL schemes, the YSU
440 and ACM2 schemes, are the foci of this study since they produced the most and least amount of
441 precipitation among PBL schemes examined. Our results serve to disentangle the turbulence –
442 cloud - precipitation processes over the Amazon and reveal root causes for the sensitivity to PBL
443 schemes, which is a prerequisite for future model improvement. During daytime, while the free-
444 troposphere clouds simulated by YSU dissipate due to solar heating, clouds simulated by ACM2
445 maintains through the day because of enhanced moisture supply due to enhanced *PBL-free-*
446 *troposphere* relay transport process: step 1, enhanced vertical mixing within PBL simulated by
447 ACM2 transports surface moisture to the PBL top where clouds first form, and step 2, enhanced
448 free-troposphere mixing feeds the moisture into the free-troposphere cloud deck. Due to the

449 thicker cloud deck over the Amazon simulated by ACM2, surface radiative heating is reduced and

450 consequently CAPE is reduced. As a result, precipitation is weaker from ACM2. In contrast, the

451 moisture *PBL-free-troposphere* relay transport process simulated by YSU is weaker and the clouds

452 at ~4-5 km dissipate quicker, and CAPE is therefore larger during daytime, leading to more

453 precipitation. To verify the strength of such relay transport process, more advanced observations

454 are warranted, for example, of long-term vertical profiles of cloud mixing ratios. To correctly

455 simulate clouds and precipitation, model performance of reproducing such a moisture relay

456 transport process needs to be carefully evaluated.

457 Two key parameters dictating the vertical mixing in the YSU and ACM2 schemes are

458 identified, which are p, an exponent in the polynomial function determining boundary layer

459 vertical mixing and λ, the asymptotic length scale dictating free-troposphere mixing. Sensitivity

460 simulations with altered p, λ, and other treatments within YSU and ACM2 confirm the sensitivity

461 of precipitation to the mixing strength. The free-troposphere mixing in presence of clouds become

462 prominent (which is otherwise weak) because of reduced moist static stability and the difference

463 in free-troposphere mixing appears to explain more of the sensitivity to the YSU and ACM2 PBL

464 schemes. The turbulent mixing and cloud relationship over the Amazon simulated with ACM2

465 suggests strong positive feedback through which regions of lower troposphere clouds create

466 conditions favorable for daytime cloud maintenance. Such feedback is weaker with YSU, which

467 leads to daytime breakup of free-troposphere clouds.

468 The above results regarding the turbulence-clouds-precipitation processes and their

469 parameterizations have important implications to the understanding and accurate prediction of

470 weather, climate, as well as air quality over the Amazon region that is humid, cloudy and rich in

471 precipitation. South America is experiencing an increasing trend in summer precipitation, and

472 such a trend is also projected by climate models (Vera et al., 2006). Given the negative cloud-

473 precipitation correlation seen in this study for the Amazon region, such a precipitation trend may

474 imply a decreasing trend of cloud cover in the region. Correct representation of turbulence mixing-

475 cloud-radiation interactions within weather and climate models is clearly critical for accurate

476 simulation/prediction of precipitation and water cycles.

477 Though not shown here, since simulated precipitation is weaker with ACM2, the

478 corresponding tropospheric upward motion is also weaker , so stronger easterly winds impinge on

479 the east side of Andes and are diverted southward to form a stronger southward LLJ east of Andes.

480 Thus, the simulated strength of Amazonian precipitation is closely linked to the strength of LLJ
481 east of Andes, which may have implications for the simulation of downstream atmospheric
482 environments including temperature and humidity conditions and air quality (Hu et al., 2013b; Hu
483 et al., 2013c; Klein et al., 2014). These are topics for future studies.

484
485

501 *Data Availability Statement.*

502   The ERA5 reanalysis data are available at https://doi.org/10.5065/BH6N-5N20.   GPM   IMERG
503 Final Precipitation dataset is available at https://doi.org/10.5067/GPM/IMERGDF/DAY/06 (last
504 access: 12 November 2020). CMORPH dataset is available at
505 https://ftp.cpc.ncep.noaa.gov/precip/CMORPH_V1.0/CRT/8km-30min (last access: 12 November
506 2020). Figures in this manuscript are produced using the NCAR Command Language (Version
507 6.6.2) [Software]. (2019). Boulder, Colorado: UCAR/NCAR/CISL/TDD.
508 http://dx.doi.org/10.5065/D6WD3XH5 . Model data produced from this study have been archived
509 at CAPS website https://caps.ou.edu/micronet/Regionalclimate.html

References

Adebiyi, A. A., Zuidema, P., Chang, I., Burton, S. P., & Cairns, B. (2020). Mid-level clouds are frequent above the southeast Atlantic stratocumulus clouds. *Atmos. Chem. Phys., 20*(18), 11025-11043. 10.5194/acp-20-11025-2020

Angevine, W. M., Eddington, L., Durkee, K., Fairall, C., Bianco, L., & Brioude, J. (2012). Meteorological Model Evaluation for CalNex 2010. *Monthly Weather Review, 140*(12), 3885-3906. 10.1175/Mwr-D-12-00042.1

Angevine, W. M., Jiang, H. L., & Mauritsen, T. (2010). Performance of an Eddy Diffusivity-Mass Flux Scheme for Shallow Cumulus Boundary Layers. *Monthly Weather Review, 138*(7), 2895-2912. 10.1175/2010mwr3142.1

Barber, K. A., Burleyson, C. D., Feng, Z., & Hagos, S. M. (2022). The Influence of Shallow Cloud Populations on Transitions to Deep Convection in the Amazon. *Journal of the Atmospheric Sciences, 79*(3), 723-743. 10.1175/jas-d-21-0141.1

Beare, R. J., MacVean, M. K., Holtslag, A. A. M., Cuxart, J., Esau, I., Golaz, J. C., . . . Sullivan, P. (2006). An intercomparison of large-eddy simulations of the stable boundary layer. *Boundary-Layer Meteorology, 118*(2), 247-272. 10.1007/s10546-004-2820-6

Bright, D. R., & Mullen, S. L. (2002). The sensitivity of the numerical simulation of the southwest monsoon boundary layer to the choice of PBL turbulence parameterization in MM5. *Weather and Forecasting, 17*(1), 99-114. Doi 10.1175/1520-0434(2002)017<0099:Tsotns>2.0.Co;2

Burleyson, C. D., & Yuter, S. E. (2015). Patterns of Diurnal Marine Stratocumulus Cloud Fraction Variability. *Journal of Applied Meteorology and Climatology, 54*(4), 847-866. 10.1175/jamc-d-14-0178.1

Chakraborty, S., Jiang, J. H., Su, H., & Fu, R. (2020). Deep Convective Evolution From Shallow Clouds Over the Amazon and Congo Rainforests. *Journal of Geophysical Research: Atmospheres, 125*(1), e2019JD030962. https://doi.org/10.1029/2019JD030962

Chakraborty, S., Schiro, K. A., Fu, R., & Neelin, J. D. (2018). On the role of aerosols, humidity, and vertical wind shear in the transition of shallow-to-deep convection at the Green Ocean Amazon 2014/5 site. *Atmos. Chem. Phys., 18*(15), 11135-11148. 10.5194/acp-18-11135-2018

Chen, F., & Zhang, Y. (2009). On the coupling strength between the land surface and the atmosphere: From viewpoint of surface exchange coefficients. *Geophysical Research Letters, 36*. L10404, 10.1029/2009gl037980

Chen, M., Huang, Y., Li, Z., Larico, A. J. M., Xue, M., Hong, Y., . . . Morales, I. Y. (2022). Cross-Examining Precipitation Products by Rain Gauge, Remote Sensing, and WRF Simulations over a South American Region across the Pacific Coast and Andes. *Atmosphere, 13*(10), 1666.

Clark, A. J., Coniglio, M. C., Coffer, B. E., Thompson, G., Xue, M., & Kong, F. Y. (2015). Sensitivity of 24-h Forecast Dryline Position and Structure to Boundary Layer Parameterizations in Convection-Allowing WRF Model Simulations. *Weather and Forecasting, 30*(3), 613-638. 10.1175/Waf-D-14-00078.1

Cohen, A. E., Cavallo, S. M., Coniglio, M. C., & Brooks, H. E. (2015). A Review of Planetary Boundary Layer Parameterization Schemes and Their Sensitivity in Simulating Southeastern US Cold Season Severe Weather Environments. *Weather and Forecasting, 30*(3), 591-612. 10.1175/Waf-D-14-00105.1

Coniglio, M. C., Correia, J., Marsh, P. T., & Kong, F. Y. (2013). Verification of Convection-Allowing WRF Model Forecasts of the Planetary Boundary Layer Using Sounding Observations. *Weather and Forecasting, 28*(3), 842-862. 10.1175/Waf-D-12-00103.1

Cuxart, J., Holtslag, A. A. M., Beare, R. J., Bazile, E., Beljaars, A., Cheng, A., . . . Xu, K. M. (2006). Single-column model intercomparison for a stably stratified atmospheric boundary layer. *Boundary-Layer Meteorology, 118*(2), 273-303. 10.1007/s10546-005-3780-1

Durran, D. R., & Klemp, J. B. (1982). On the Effects of Moisture on the Brunt-Väisälä Frequency. *Journal of Atmospheric Sciences, 39*(10), 2152-2158. 10.1175/1520-0469(1982)039<2152:Oteomo>2.0.Co;2

Fu, R., Zhu, B., & Dickinson, R. E. (1999). How Do Atmosphere and Land Surface Influence Seasonal Changes of Convection in the Tropical Amazon? *Journal of Climate, 12*(5), 1306-1321. 10.1175/1520-0442(1999)012<1306:Hdaals>2.0.Co;2

Giangrande, S. E., Feng, Z., Jensen, M. P., Comstock, J. M., Johnson, K. L., Toto, T., . . . Martin, S. T. (2017). Cloud characteristics, thermodynamic controls and radiative impacts during the Observations and Modeling of the Green Ocean Amazon (GoAmazon2014/5) experiment. *Atmos. Chem. Phys., 17*(23), 14519-14541. 10.5194/acp-17-14519-2017

Giangrande, S. E., Wang, D., & Mechem, D. B. (2020). Cloud regimes over the Amazon Basin: perspectives from the GoAmazon2014/5 campaign. *Atmos. Chem. Phys., 20*(12), 7489-7507. 10.5194/acp-20-7489-2020

Gunwani, P., & Mohan, M. (2017). Sensitivity of WRF model estimates to various PBL parameterizations in different climatic zones over India. *Atmospheric Research, 194*, 43-65. https://doi.org/10.1016/j.atmosres.2017.04.026

Hersbach, H., Bell, B., Berrisford, P., Hirahara, S., Horányi, A., Muñoz-Sabater, J., . . . Thépaut, J.-N. (2020). The ERA5 global reanalysis. *Quarterly Journal of the Royal Meteorological Society, 146*(730), 1999-2049. https://doi.org/10.1002/qj.3803

Hong, S. Y., Noh, Y., & Dudhia, J. (2006). A new vertical diffusion package with an explicit treatment of entrainment processes. *Monthly Weather Review, 134*(9), 2318-2341. Doi 10.1175/Mwr3199.1

Hu, X.-M., Doughty, D. C., Sanchez, K. J., Joseph, E., & Fuentes, J. D. (2012). Ozone variability in the atmospheric boundary layer in Maryland and its implications for vertical transport model. *Atmospheric Environment, 46*, 354-364. 10.1016/j.atmosenv.2011.09.054

Hu, X.-M., Klein, P. M., & Xue, M. (2013a). Evaluation of the updated YSU planetary boundary layer scheme within WRF for wind resource and air quality assessments. *Journal of Geophysical Research-Atmospheres, 118*(18), 10490-10505. 10.1002/jgrd.50823

Hu, X.-M., Klein, P. M., Xue, M., Lundquist, J. K., Zhang, F., & Qi, Y. (2013b). Impact of Low-Level Jets on the Nocturnal Urban Heat Island Intensity in Oklahoma City. *Journal of Applied Meteorology and Climatology, 52*(8), 1779-1802. 10.1175/jamc-d-12-0256.1

Hu, X.-M., Klein, P. M., Xue, M., Zhang, F., Doughty, D. C., Forkel, R., . . . Fuentes, J. D. (2013c). Impact of the vertical mixing induced by low-level jets on boundary layer ozone concentration. *Atmospheric Environment, 70*, 123-130. 10.1016/j.atmosenv.2012.12.046

Hu, X.-M., Nielsen-Gammon, J. W., & Zhang, F. Q. (2010a). Evaluation of Three Planetary Boundary Layer Schemes in the WRF Model. *Journal of Applied Meteorology and Climatology, 49*(9), 1831-1844. 10.1175/2010jamc2432.1

Hu, X.-M., Xue, M., & Li, X. (2019). The Use of High-Resolution Sounding Data to Evaluate and Optimize Nonlocal PBL Schemes for Simulating the Slightly Stable Upper

601   Convective Boundary Layer. *Monthly Weather Review, 147*(10), 3825-3841.
602   10.1175/mwr-d-19-0085.1
603 Hu, X.-M., Xue, M., McPherson, R. A., Martin, E., Rosendahl, D. H., & Qiao, L. (2018).
604   Precipitation Dynamical Downscaling Over the Great Plains. *Journal of Advances in*
605   *Modeling Earth Systems, 10*(2), 421-447. 10.1002/2017ms001154
606 Hu, X.-M., Zhang, F., & Nielsen-Gammon, J. W. (2010b). Ensemble-based simultaneous state
607   and parameter estimation for treatment of mesoscale model error: A real-data study.
608   *Geophysical Research Letters, 37*. L08802, 10.1029/2010gl043017
609 Huang, H. Y., Hall, A., & Teixeira, J. (2013). Evaluation of the WRF PBL Parameterizations for
610   Marine Boundary Layer Clouds: Cumulus and Stratocumulus. *Monthly Weather Review,*
611   *141*(7), 2265-2271. 10.1175/Mwr-D-12-00292.1
612 Huang, Y., Xue, M., Hu, X.-M., Martin, E. R., Novoa, H., McPherson, R. A., . . . Morales, I. Y.
613   (2022). *Characteristics of Precipitation and MCS over the Peruvian Central Andes based*
614   *on Convection-Permitting Simulations.* Paper presented at the AGU fall meeting,
615   Chicago, IL, https://agu.confex.com/agu/fm22/meetingapp.cgi/Person/177979.
616 Huffman, G. J., E.F. Stocker, D.T. Bolvin, Nelkin, E. J., & Tan, J. (2019). GPM IMERG Final
617   Precipitation L3 1 day 0.1 degree x 0.1 degree V06 (Publication no.
618   https://doi.org/10.5067/GPM/IMERGDF/DAY/06). Retrieved Nov. 2022
619 Iacono, M. J., Delamere, J. S., Mlawer, E. J., Shephard, M. W., Clough, S. A., & Collins, W. D.
620   (2008). Radiative forcing by long-lived greenhouse gases: Calculations with the AER
621   radiative transfer models. *Journal of Geophysical Research: Atmospheres, 113*(D13).
622   https://doi.org/10.1029/2008JD009944
623 Jankov, I., Gallus, W. A., Segal, M., Shaw, B., & Koch, S. E. (2005). The impact of different
624   WRF model physical parameterizations and their interactions on warm season MCS
625   rainfall. *Weather and Forecasting, 20*(6), 1048-1060. Doi 10.1175/Waf888.1
626 Jankov, I., Schultz, P. J., Anderson, C. J., & Koch, S. E. (2007). The Impact of Different
627   Physical Parameterizations and Their Interactions on Cold Season QPF in the American
628   River Basin. *Journal of Hydrometeorology, 8*(5), 1141-1151. 10.1175/jhm630.1
629 Jiménez, P. A., Dudhia, J., González-Rouco, J. F., Navarro, J., Montávez, J. P., & García-
630   Bustamante, E. (2012). A Revised Scheme for the WRF Surface Layer Formulation.
631   *Monthly Weather Review, 140*(3), 898-918. 10.1175/mwr-d-11-00056.1
632 Joyce, R. J., Janowiak, J. E., Arkin, P. A., & Xie, P. (2004). CMORPH: A Method that Produces
633   Global Precipitation Estimates from Passive Microwave and Infrared Data at High
634   Spatial and Temporal Resolution. *Journal of Hydrometeorology, 5*(3), 487-503.
635   10.1175/1525-7541(2004)005<0487:Camtpg>2.0.Co;2
636 Kay, J. E., Bourdages, L., Miller, N. B., Morrison, A., Yettella, V., Chepfer, H., & Eaton, B.
637   (2016). Evaluating and improving cloud phase in the Community Atmosphere Model
638   version 5 using spaceborne lidar observations. *Journal of Geophysical Research:*
639   *Atmospheres, 121*(8), 4162-4176. https://doi.org/10.1002/2015JD024699
640 Kay, J. E., Hillman, B. R., Klein, S. A., Zhang, Y., Medeiros, B., Pincus, R., . . . Ackerman, T. P.
641   (2012). Exposing Global Cloud Biases in the Community Atmosphere Model (CAM)
642   Using Satellite Observations and Their Corresponding Instrument Simulators. *Journal of*
643   *Climate, 25*(15), 5190-5207. 10.1175/jcli-d-11-00469.1
644 Klein, P. M., Hu, X. M., & Xue, M. (2014). Impacts of Mixing Processes in Nocturnal
645   Atmospheric Boundary Layer on Urban Ozone Concentrations. *Boundary-Layer*
646   *Meteorology, 150*(1), 107-130. 10.1007/s10546-013-9864-4

647 Langenbrunner, B., Pritchard, M. S., Kooperman, G. J., & Randerson, J. T. (2019). Why Does
648   Amazon Precipitation Decrease When Tropical Forests Respond to Increasing CO_2?
649   *Earth's Future, 7*(4), 450-468. https://doi.org/10.1029/2018EF001026
650 Li, X. L., & Pu, Z. X. (2008). Sensitivity of Numerical Simulation of Early Rapid Intensification
651   of Hurricane Emily (2005) to Cloud Microphysical and Planetary Boundary Layer
652   Parameterizations. *Monthly Weather Review, 136*(12), 4819-4838.
653   10.1175/2008mwr2366.1
654 Lilly, D. K. (1968). Models of Cloud-Topped Mixed Layers under a Strong Inversion. *Quarterly*
655   *Journal of the Royal Meteorological Society, 94*(401), 292-&. DOI
656   10.1002/qj.49709440106
657 Liu, C., Ikeda, K., Rasmussen, R., Dominguez, F., Prein, A. F., Dudhia, J., & Chen, F. (2022).
658   *An Overview of Two-Decade-Long Convection Permitting Regional Climate*
659   *Downscaling over the Continental South America.* Paper presented at the AGU fall
660   meeting, Chicago, IL, https://agu.confex.com/agu/fm22/meetingapp.cgi/Paper/1115319.
661 Liu, M., & Carroll, J. J. (1996). A high-resolution air pollution model suitable for dispersion
662   studies in complex terrain. *Monthly Weather Review, 124*(10), 2396-2409. Doi
663   10.1175/1520-0493(1996)124<2396:Ahrapm>2.0.Co;2
664 Lu, X., & Wang, X. (2019). Improving Hurricane Analyses and Predictions with TCI, IFEX
665   Field Campaign Observations, and CIMSS AMVs Using the Advanced Hybrid Data
666   Assimilation System for HWRF. Part I: What is Missing to Capture the Rapid
667   Intensification of Hurricane Patricia (2015) when HWRF is already Initialized with a
668   More Realistic Analysis? *Monthly Weather Review, 147*(4), 1351-1373. 10.1175/mwr-d-
669   18-0202.1
670 Miguez-Macho, G., Stenchikov, G. L., & Robock, A. (2004). Spectral nudging to eliminate the
671   effects of domain position and geometry in regional climate model simulations. *Journal*
672   *of Geophysical Research-Atmospheres, 109*(D13). D13104, 10.1029/2003jd004495
673 Miguez-Macho, G., Stenchikov, G. L., & Robock, A. (2005). Regional climate simulations over
674   North America: Interaction of local processes with improved large-scale flow. *Journal of*
675   *Climate, 18*(8), 1227-1246. Doi 10.1175/Jcli3369.1
676 Nakanishi, M., & Niino, H. (2006). An Improved Mellor–Yamada Level-3 Model: Its Numerical
677   Stability and Application to a Regional Prediction of Advection Fog. *Boundary-Layer*
678   *Meteorology, 119*(2), 397-407. 10.1007/s10546-005-9030-8
679 Nielsen-Gammon, J. W., Hu, X.-M., Zhang, F., & Pleim, J. E. (2010). Evaluation of Planetary
680   Boundary Layer Scheme Sensitivities for the Purpose of Parameter Estimation. *Monthly*
681   *Weather Review, 138*(9), 3400-3417. 10.1175/2010mwr3292.1
682 Noh, Y., Cheon, W. G., Hong, S. Y., & Raasch, S. (2003). Improvement of the K-profile model
683   for the planetary boundary layer based on large eddy simulation data. *Boundary-Layer*
684   *Meteorology, 107*(2), 401-427. Doi 10.1023/A:1022146015946
685 Olson, J. B., Kenyon, J. S., Angevine, W. A., Brown, J. M., Pagowski, M., & Sušelj, K. (2019a).
686   A Description of the MYNN-EDMF Scheme and the Coupling to Other Components in
687   WRF–ARW. https://doi.org/10.25923/n9wm-be49
688 Olson, J. B., Kenyon, J. S., Djalalova, I., Bianco, L., Turner, D. D., Pichugina, Y., . . . Cline, J.
689   (2019b). Improving Wind Energy Forecasting through Numerical Weather Prediction
690   Model Development. *Bulletin of the American Meteorological Society, 100*(11), 2201-
691   2220. 10.1175/bams-d-18-0040.1

Painemal, D., Xu, K.-M., Cheng, A., Minnis, P., & Palikonda, R. (2015). Mean Structure and Diurnal Cycle of Southeast Atlantic Boundary Layer Clouds: Insights from Satellite Observations and Multiscale Modeling Framework Simulations. *Journal of Climate, 28*(1), 324-341. 10.1175/jcli-d-14-00368.1

Pergaud, J., Masson, V., Malardel, S., & Couvreux, F. (2009). A parameterization of dry thermals and shallow cumuli for mesoscale numerical weather prediction. *Bound.-Layer Meteor., 132*, 83-106.

Pleim, J. E. (2007). A combined local and nonlocal closure model for the atmospheric boundary layer. Part I: Model description and testing. *Journal of Applied Meteorology and Climatology, 46*(9), 1383-1395. 10.1175/Jam2539.1

Prein, A. F., Ge, M., Valle, A. R., Wang, D., & Giangrande, S. E. (2022). Towards a Unified Setup to Simulate Mid-Latitude and Tropical Mesoscale Convective Systems at Kilometer-Scales. *Earth and Space Science, 9*(8), e2022EA002295. https://doi.org/10.1029/2022EA002295

Prein, A. F., Langhans, W., Fosser, G., Ferrone, A., Ban, N., Goergen, K., . . . Leung, R. (2015). A review on regional convection-permitting climate modeling: Demonstrations, prospects, and challenges. *Reviews of Geophysics, 53*(2), 323-361.

Prein, A. F., Rasmussen, R. M., Ikeda, K., Liu, C., Clark, M. P., & Holland, G. J. (2017). The future intensification of hourly precipitation extremes. *Nature Clim. Change, 7*(1), 48-52. 10.1038/nclimate3168, http://www.nature.com/nclimate/journal/v7/n1/abs/nclimate3168.html#supplementary-information

Shin, H. H., & Hong, S. Y. (2011). Intercomparison of Planetary Boundary-Layer Parametrizations in the WRF Model for a Single Day from CASES-99. *Boundary-Layer Meteorology, 139*(2), 261-281. 10.1007/s10546-010-9583-z

Skamarock, W. C., & Klemp, J. B. (2008). A time-split nonhydrostatic atmospheric model for weather research and forecasting applications. *Journal of Computational Physics, 227*(7), 3465-3485. http://dx.doi.org/10.1016/j.jcp.2007.01.037

Skamarock, W. C., Klemp, J. B., Dudhia, J., Gill, D. O., Liu, Z., Berner, J., . . . Huang, X.-y. (2021). *A Description of the Advanced Research WRF Model Version 4.3*. (NCAR/TN-556+STR). Retrieved from http://dx.doi.org/10.5065/1dfh-6p97.

Sun, X. G., Xue, M., Brotzge, J., McPherson, R. A., Hu, X. M., & Yang, X. Q. (2016). An evaluation of dynamical downscaling of Central Plains summer precipitation using a WRF-based regional climate model at a convection-permitting 4km resolution. *Journal of Geophysical Research-Atmospheres, 121*(23), 13801-13825. 10.1002/2016jd024796

Supinie, T. A., Park, J., Snook, N., Hu, X. M., Brewster, K. A., Xue, M., & Carley, J. R. (2022). Cool-Season Evaluation of FV3-LAM-Based CONUS-Scale Forecasts with Physics Configurations of Experimental RRFS Ensembles. *Monthly Weather Review, 150*(9), 2379-2398. 10.1175/mwr-d-21-0331.1

Tai, S.-L., Feng, Z., Ma, P.-L., Schumacher, C., & Fast, J. D. (2021). Representations of Precipitation Diurnal Cycle in the Amazon as Simulated by Observationally Constrained Cloud-System Resolving and Global Climate Models. *Journal of Advances in Modeling Earth Systems, 13*(11), e2021MS002586. https://doi.org/10.1029/2021MS002586

Thompson, G., Field, P. R., Rasmussen, R. M., & Hall, W. D. (2008). Explicit Forecasts of Winter Precipitation Using an Improved Bulk Microphysics Scheme. Part II:

Implementation of a New Snow Parameterization. *Monthly Weather Review, 136*(12), 5095-5115. 10.1175/2008mwr2387.1

Tiedtke, M. (1989). A Comprehensive Mass Flux Scheme for Cumulus Parameterization in Large-Scale Models. *Monthly Weather Review, 117*(8), 1779-1800. Doi 10.1175/1520-0493(1989)117<1779:Acmfsf>2.0.Co;2

Troen, I., & Mahrt, L. (1986). A Simple-Model of the Atmospheric Boundary-Layer - Sensitivity to Surface Evaporation. *Boundary-Layer Meteorology, 37*(1-2), 129-148. Doi 10.1007/Bf00122760

Vera, C., Silvestri, G., Liebmann, B., & González, P. (2006). Climate change scenarios for seasonal precipitation in South America from IPCC-AR4 models. *Geophysical Research Letters, 33*(13). https://doi.org/10.1029/2006GL025759

Wang, J. L., & Kotamarthi, V. R. (2013). Assessment of Dynamical Downscaling in Near-Surface Fields with Different Spectral Nudging Approaches Using the Nested Regional Climate Model (NRCM). *Journal of Applied Meteorology and Climatology, 52*(7), 1576-1591. 10.1175/Jamc-D-12-0302.1

Wang, J. X., & Hu, X. M. (2021). Evaluating the Performance of WRF Urban Schemes and PBL Schemes over Dallas-Fort Worth during a Dry Summer and a Wet Summer. *Journal of Applied Meteorology and Climatology, 60*(6), 779-798. 10.1175/Jamc-D-19-0195.1

Wang, W. G., Shen, X. Y., & Huang, W. Y. (2016). A Comparison of Boundary-Layer Characteristics Simulated Using Different Parametrization Schemes. *Boundary-Layer Meteorology, 161*(2), 375-403. 10.1007/s10546-016-0175-4

Wright, J. S., Fu, R., Worden, J. R., Chakraborty, S., Clinton, N. E., Risi, C., . . . Yin, L. (2017). Rainforest-initiated wet season onset over the southern Amazon. *Proceedings of the National Academy of Sciences, 114*(32), 8481-8486. doi:10.1073/pnas.1621516114

Wu, M., Lee, J.-E., Wang, D., & Salameh, M. (2021a). Suppressed Daytime Convection Over the Amazon River. *Journal of Geophysical Research: Atmospheres, 126*(13), e2020JD033627. https://doi.org/10.1029/2020JD033627

Wu, Z., Li, Y., Li, X., Hu, X.-M., Zhou, G., & Deng, C. (2021b). Influence of Different Planetary Boundary Layer Parameterization Schemes on the Simulation of Precipitation Caused by Southwest China Vortex in Sichuan Basin Based on the WRF Model. *Chinese Journal of Atmospheric Sciences, 45*(1), 58. 10.3878/j.issn.1006-9895.2005.19171

Xie, B., Fung, J. C. H., Chan, A., & Lau, A. (2012). Evaluation of nonlocal and local planetary boundary layer schemes in the WRF model. *Journal of Geophysical Research: Atmospheres, 117*(D12). https://doi.org/10.1029/2011JD017080

Yang, Y., Hu, X.-M., Gao, S., & Wang, Y. (2019). Sensitivity of WRF simulations with the YSU PBL scheme to the lowest model level height for a sea fog event over the Yellow Sea. *Atmospheric Research, 215*, 253-267. https://doi.org/10.1016/j.atmosres.2018.09.004

Zhang, D., Wang, Z., & Liu, D. (2010). A global view of midlevel liquid-layer topped stratiform cloud distribution and phase partition from CALIPSO and CloudSat measurements. *Journal of Geophysical Research: Atmospheres, 115*(D4). https://doi.org/10.1029/2009JD012143

Zhang, Y., Jiang, Y., & Tan, B. (2013). Influences of different PBL schemes on secondary eyewall formation and eyewall replacement cycle in simulated Typhoon Sinlaku (2008). *Acta Meteorologica Sinica, 27*, 322-334. 10.1007/s13351-013-0312-7

Zhu, P., Hazelton, A., Zhang, Z., Marks, F. D., & Tallapragada, V. (2021). The Role of Eyewall Turbulent Transport in the Pathway to Intensification of Tropical Cyclones. *Journal of*

783   *Geophysical Research: Atmospheres, 126*(17), e2021JD034983.

784   https://doi.org/10.1029/2021JD034983

785 Zhu, P., Tyner, B., Zhang, J. A., Aligo, E., Gopalakrishnan, S., Marks, F. D., . . . Tallapragada,

786   V. (2019). Role of eyewall and rainband eddy forcing in tropical cyclone intensification.

787   *Atmos. Chem. Phys., 19*(22), 14289-14310. 10.5194/acp-19-14289-2019

788

789

790 Table 1. Model configuration for sensitivity simulations modifying parameters and treatments in
791 the YSU and ACM2 PBL schemes. p is an exponent in the polynomial function determining
792 vertical mixing strength in the PBL, λ is the asymptotic length scale.

PBL	Grid spacings	Experiment name	Changed parameters/treatments
YSU	15 km	YSU	$p=2$ (default)
		YSUp.5	$p=0.5$
		YSUuseACM2free	Use free troposphere treatment from ACM2
		YSUp.5useACM2free	$p=0.5$ & use free troposphere treatment from ACM2
	3km	3kmYSU	$p=2$ (default)
		3kmYSUp.5	$p=0.5$
		3kmYSUp.5useACM2free	$p=0.5$ & use free troposphere treatment from ACM2
ACM2	15 km	ACM2	$\lambda=80$ (default)
		ACM2λ30	$\lambda=30$
	3 km	3kmACM2	$\lambda=80$ (default)

793

794

795 **Figures**
796 Figure 1. Daily mean precipitation rate in Jan-Feb 2019 simulated with (a) YSU in domain 1, (b)
797 ACM2 in domain 1 with a 15 km grid spacing, (c) YSU in domain 2, (d) ACM2 in domain 2 with
798 a 3 km grid spacing, (e) single-domain YSU, (f) single-domain ACM2 with a 3 km grid spacing
799 and from (g) IMERG, (h) CMORPH data. The rectangle in (a) marks the location of the nested
800 domain.
801

802 Figure 2. Hourly mean precipitation rate at 18 UTC (14 LST) in Jan-Feb 2019 simulated with (a)
803 YSU in domain 1, (b) ACM2 in domain 1, (c) YSU in domain 2, (d) ACM2 in domain 2, (e) single-
804 domain YSU, (f) single-domain ACM2 and observed from (g) IMERG, (h) CMORPH.
805

806 Figure 3. Average surface temperature at 17 UTC in Jan-Feb 2019 from (a,c,e) YSU, (b,d,f) ACM2,
807 and (g,h,i) their difference (ACM2-YSU) in (top to bottom) different domains. The average
808 difference over land is marked at the lower-left corner in (g,h,i)
809

810 Figure 4. Average surface downward shortwave radiation at 17 UTC in Jan-Feb 2019 simulated
811 with (a,c,e) YSU, (b,d,f) ACM2, (g,h,i) their difference, and (j,k,l) column-average cloud water
812 mixing ratios in (top to bottom) different domains. The straight dash lines mark the location of
813 cross-sections in Figs. 5, 6, and 11.
814

815 Figure 5. Cross-section of cloud water over the Amazon in Jan-Feb 2019 simulated by (left) YSU
816 and (right) ACM2 at (a,b) 11, (c,d) 14, (e,f) 17, and (g,h) 21 UTC (7, 10, 13, 17 LST
817 correspondingly). The location of these cross-sections is marked in Fig. 4j
818

819   Figure 6. Cross-section of cloud water over the Amazon in Jan-Feb 2019 simulated by (a) YSU
820   and (b) ACM2, (c) $YSUp.5$, (d) $YSUuseACM2free$, (e) $YSUp.5useACM2free$, (f) ACM2λ30 at 17
821   UTC. The location of these cross-sections is marked in Fig. 4j
822
823   Figure 7. Average surface downward shortwave radiation at 17 UTC during January-February
824   2019 simulated by (a) YSU, (b) ACM2 and 4 sensitivity simulations (c) $YSUp.5$, (d)
825     $YSUuseACM2free$, (e) $YSUp.5useACM2free$, (f) ACM2λ30.
826
827   Figure 8. Average CAPE at 17 UTC during January-February 2019 simulated by (a) YSU, (b)
828   ACM2 and 4 sensitivity simulations (c) $YSUp.5$, (d) $YSUuseACM2free$, (e) $YSUp.5useACM2free$,
829   (f) ACM2λ30.
830
831   Figure 9. Mean profiles of (a) water vapor mixing ratio, (b) water vapor difference from that
832   simulated by YSU, (c) cloud water mixing ratio (QCLOUD), and (d) vertical mixing coefficient
833   (K_z) at 17 UTC during January-February 2019 at Manaus (location marked in Fig. 8b) simulated
834   by YSU, ACM2 and 4 sensitivity simulations $YSUp.5, YSUuseACM2free, YSUp.5useACM2free$,
835   ACM2λ30.
836
837   Figure 10. Average precipitation rate at 18 UTC during January-February 2019 simulated by (a)
838   YSU, (b) ACM2 and 4 sensitivity simulations (c) $YSUp.5$, (d) $YSUuseACM2free$, (e)
839     $YSUp.5useACM2free$, (f) ACM2λ30.
840
841   Figure 11. Cross-section of average noon-time cloud water mixing ratios over the Amazon in Jan-
842   Feb 2019 simulated by (a) $3kmYSU$, (b) $3kmACM2$, (c) $3kmYSUp.5$, and (d)
843     $3kmYSUp.5useACM2free$. The location of these cross-sections is marked in Fig. 4l
844
845   Figure 12. Average noon-time precipitation rate in Jan-Feb 2019 simulated by (a) $3kmYSU$, (b)
846     $3kmACM2$, (c) $3kmYSUp.5$, and (d) $3kmYSUp.5useACM2free$. The domain-averaged values are
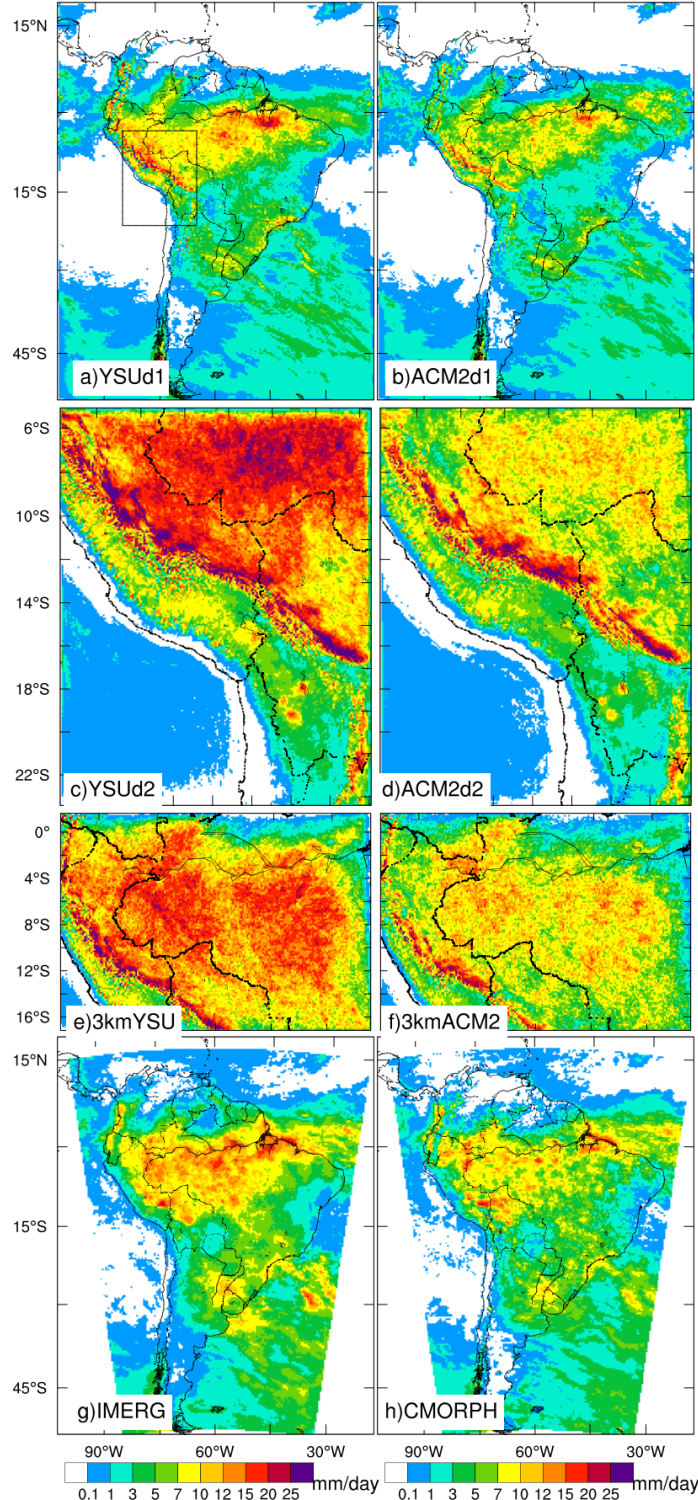847   marked.
848

Figures.

Figure 1. Daily mean precipitation rate in Jan-Feb 2019 simulated with (a) YSU in domain 1, (b) ACM2 in domain 1 with a 15 km grid spacing, (c) YSU in domain 2, (d) ACM2 in domain 2 with a 3 km grid spacing, (e) single-domain YSU, (f) single-domain ACM2 with a 3 km grid spacing and from (g) IMERG, (h) CMORPH data. The rectangle in (a) marks the location of the nested domain.
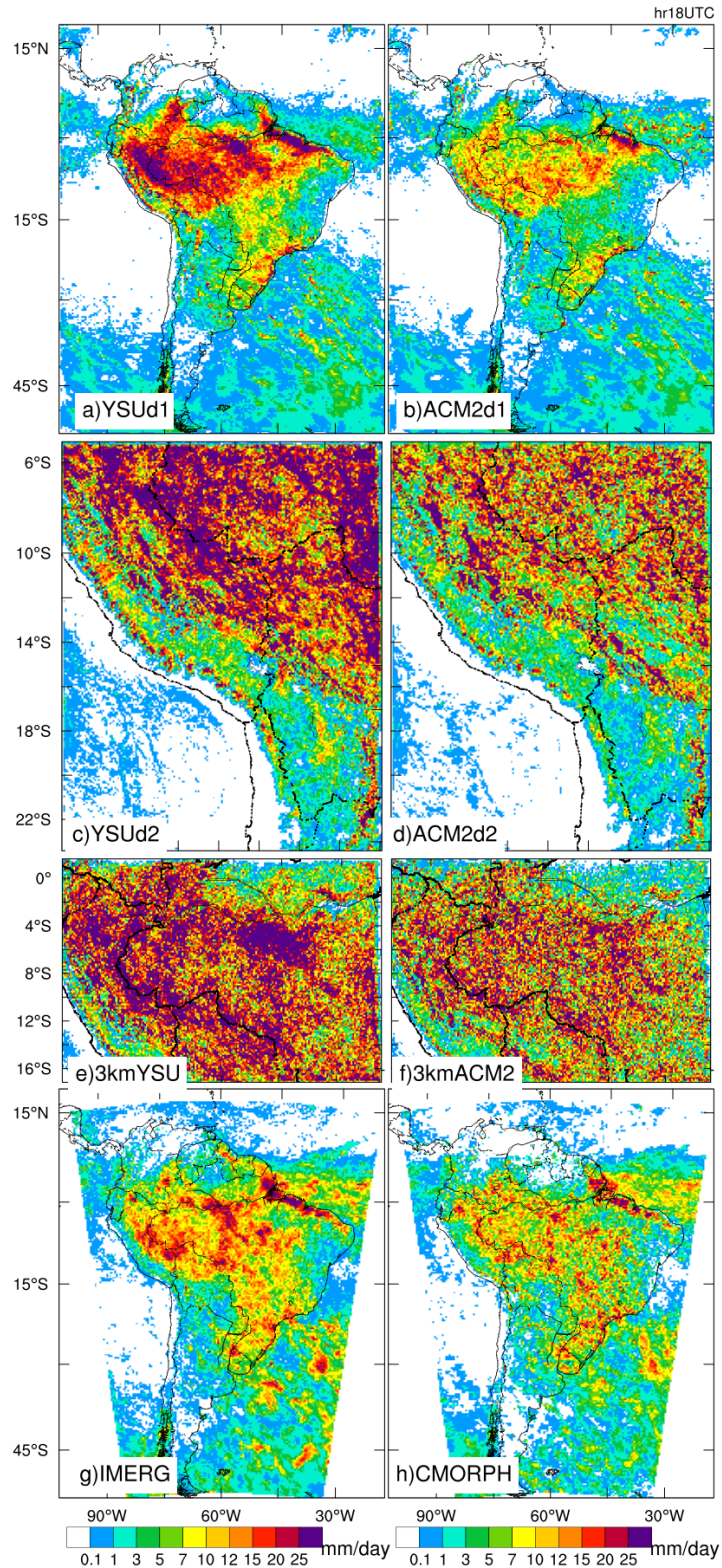
Figure 2. Hourly mean precipitation rate at 18 UTC (14 LST) in Jan-Feb 2019 simulated with (a) YSU in domain 1, (b) ACM2 in domain 1, (c) YSU in domain 2, (d) ACM2 in domain 2, (e) single-domain YSU, (f) single-domain ACM2 and observed from (g) IMERG, (h) CMORPH.

Figure 3. Average surface temperature at 17 UTC in Jan-Feb 2019 from (a,c,e) YSU, (b,d,f) ACM2, and (g,h,i) their difference (ACM2-YSU) in (top to bottom) different domains. The average difference over land is marked at the lower-left corner in (g,h,i)

Figure 4. Average surface downward shortwave radiation at 17 UTC in Jan-Feb 2019 simulated with (a,c,e) YSU, (b,d,f) ACM2, (g,h,i) their difference, and (j,k,l) column-average cloud water mixing ratios in (top to bottom) different domains. The straight dash lines mark the location of cross-sections in Figs. 5, 6, and 11.

Figure 5. Cross-section of cloud water over the Amazon in Jan-Feb 2019 simulated by (left) YSU and (right) ACM2 at (a,b) 11, (c,d) 14, (e,f) 17, and (g,h) 21 UTC (7, 10, 13, 17 LST correspondingly). The location of these cross-sections is marked in Fig. 4j

Figure 6. Cross-section of cloud water over the Amazon in Jan-Feb 2019 simulated by (a) YSU and (b) ACM2, (c) YSUp. 5, (d) YSUuseACM2free, (e) YSUp. 5useACM2free, (f) ACM2λ30 at 17 UTC. The location of these cross-sections is marked in Fig. 4j

Figure 7. Average surface downward shortwave radiation at 17 UTC during January-February 2019 simulated by (a) YSU, (b) ACM2 and 4 sensitivity simulations (c) YSUp.5, (d) YSUuseACM2free, (e) YSUp.5useACM2free, (f) ACM2λ30.
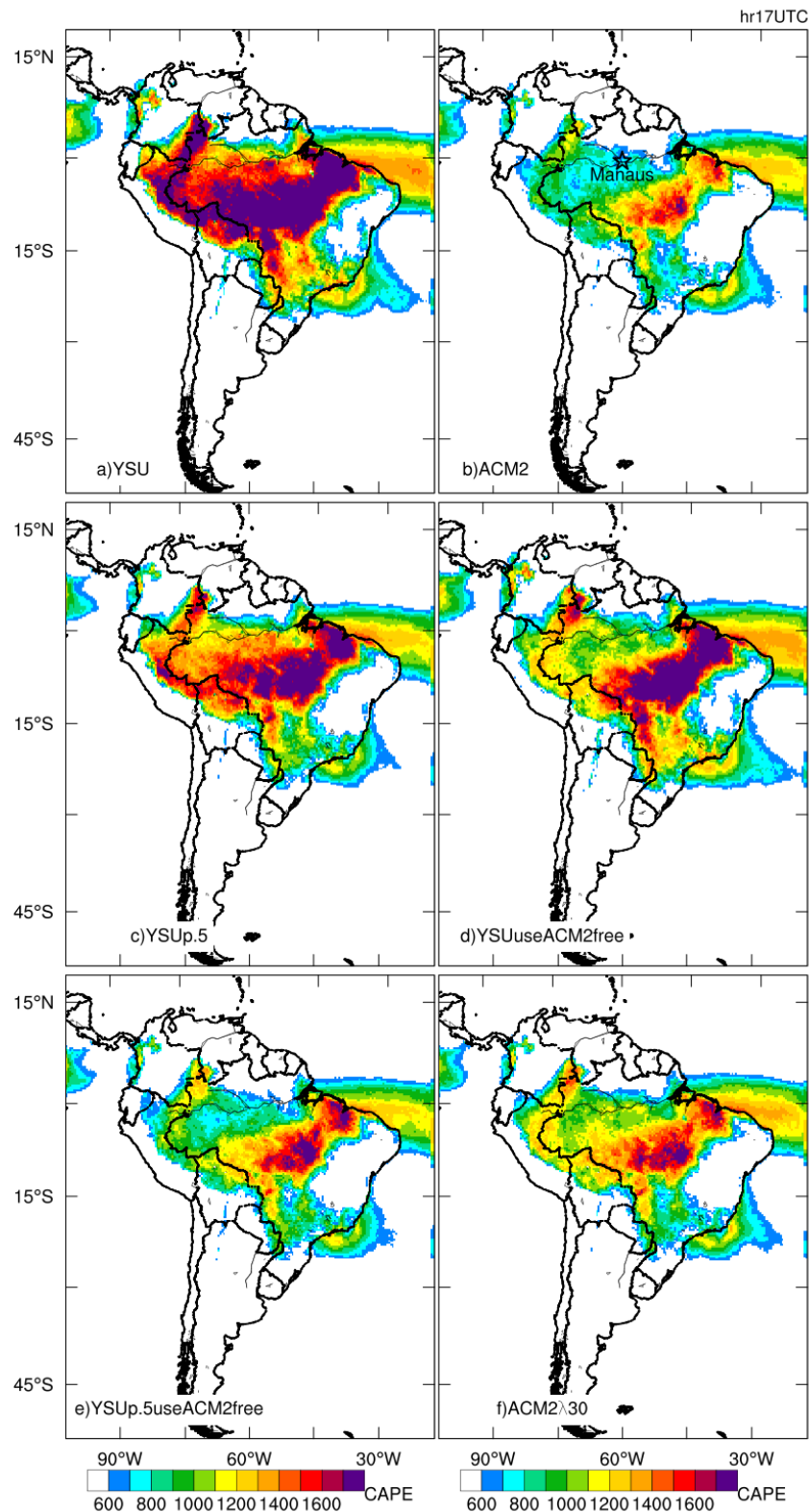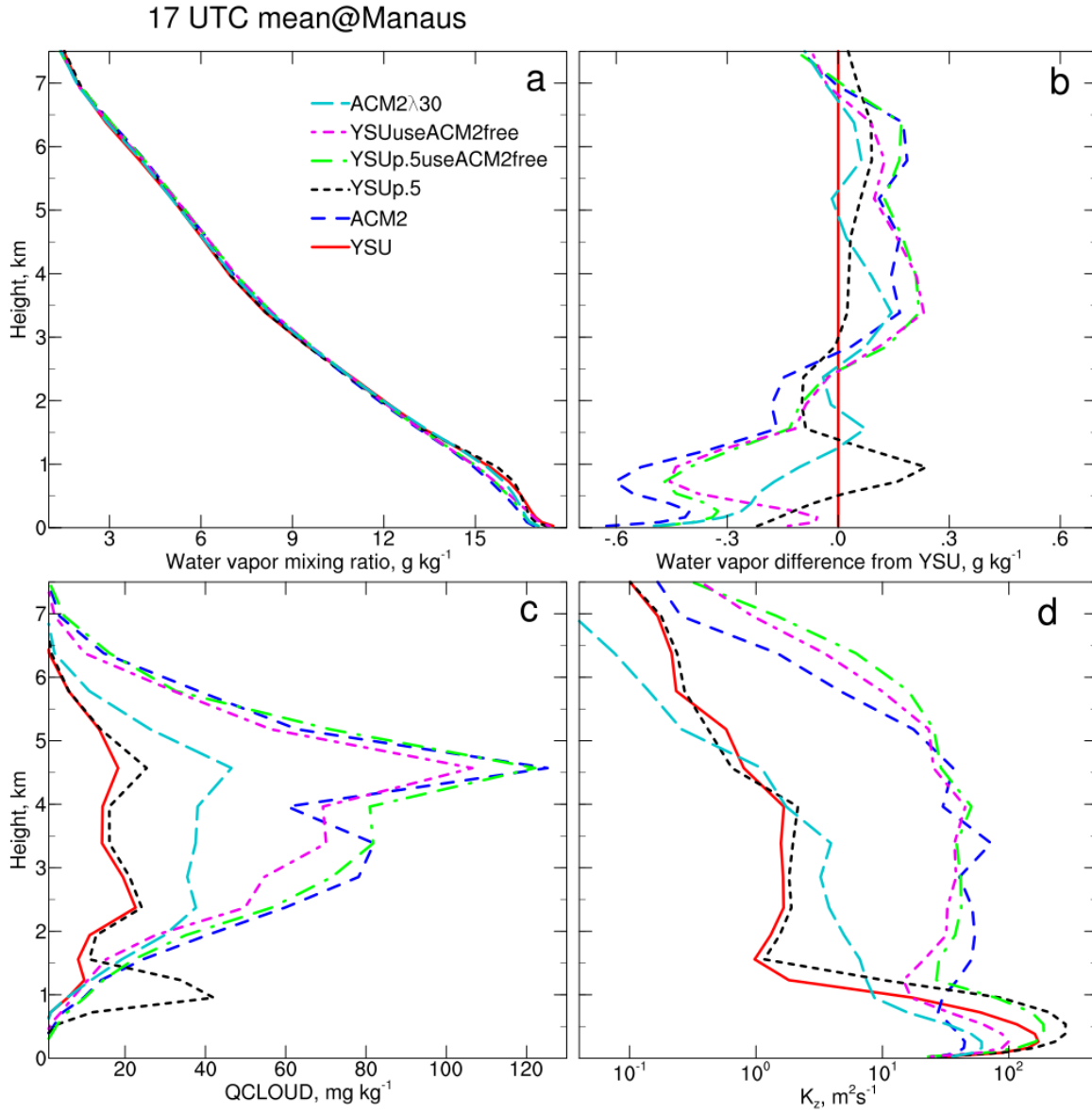
Figure 8. Average CAPE at 17 UTC during January-February 2019 simulated by (a) YSU, (b) ACM2 and 4 sensitivity simulations (c) YSUp.5, (d) YSUuseACM2free, (e) YSUp.5useACM2free, (f) ACM2λ30.

Figure 9. Mean profiles of (a) water vapor mixing ratio, (b) water vapor difference from that simulated by YSU, (c) cloud water mixing ratio (QCLOUD), and (d) vertical mixing coefficient (K_z) at 17 UTC during January-February 2019 at Manaus (location marked in Fig. 8b) simulated by YSU, ACM2 and 4 sensitivity simulations YSUp.5, YSUuseACM2free, YSUp.5useACM2free, ACM2λ30.
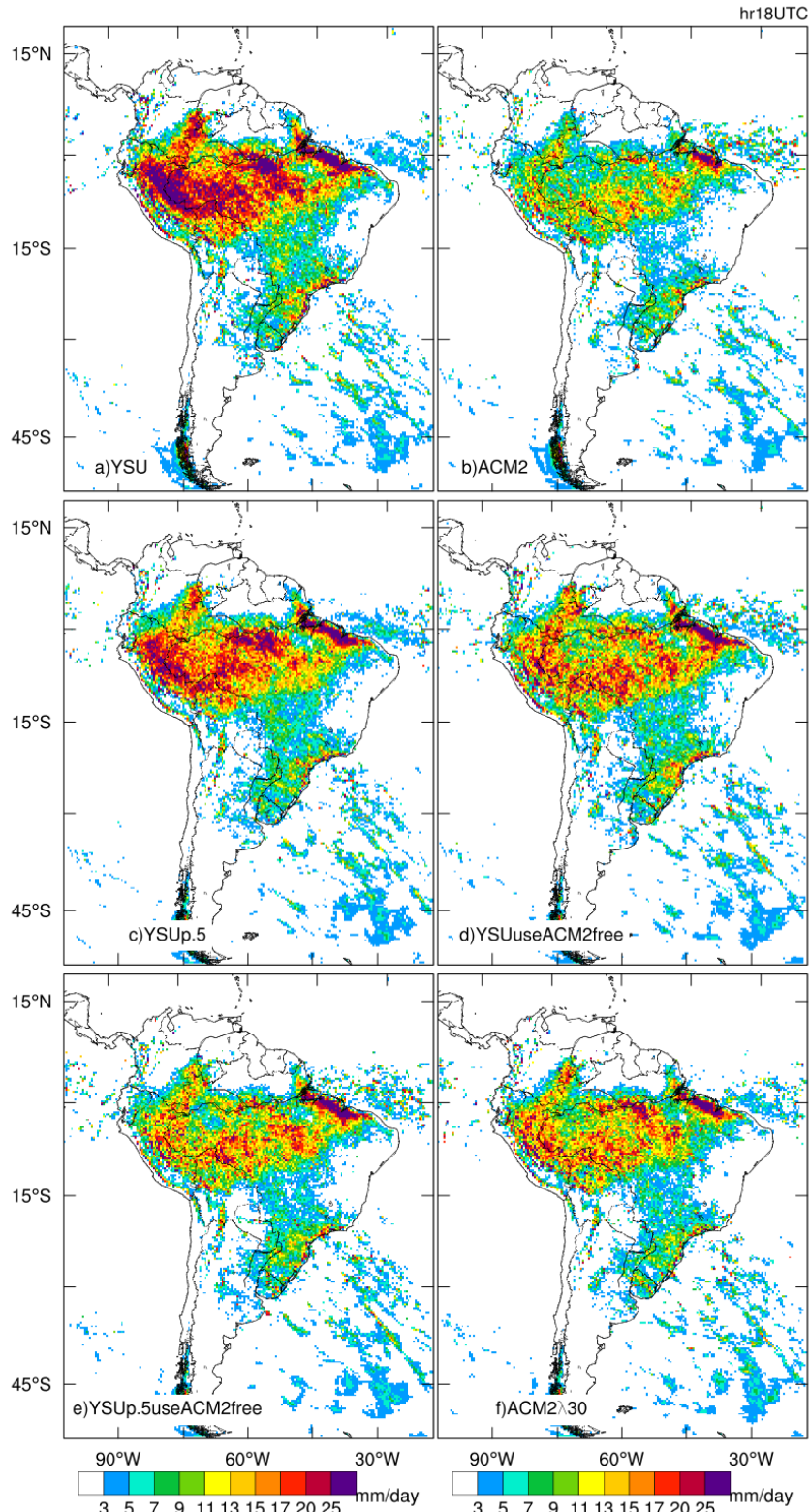
Figure 10. Average precipitation rate at 18 UTC during January-February 2019 simulated by (a) YSU, (b) ACM2 and 4 sensitivity simulations (c) YSUp.5 , (d) YSUuseACM2free , (e) YSUp.5useACM2free, (f) ACM2λ30.
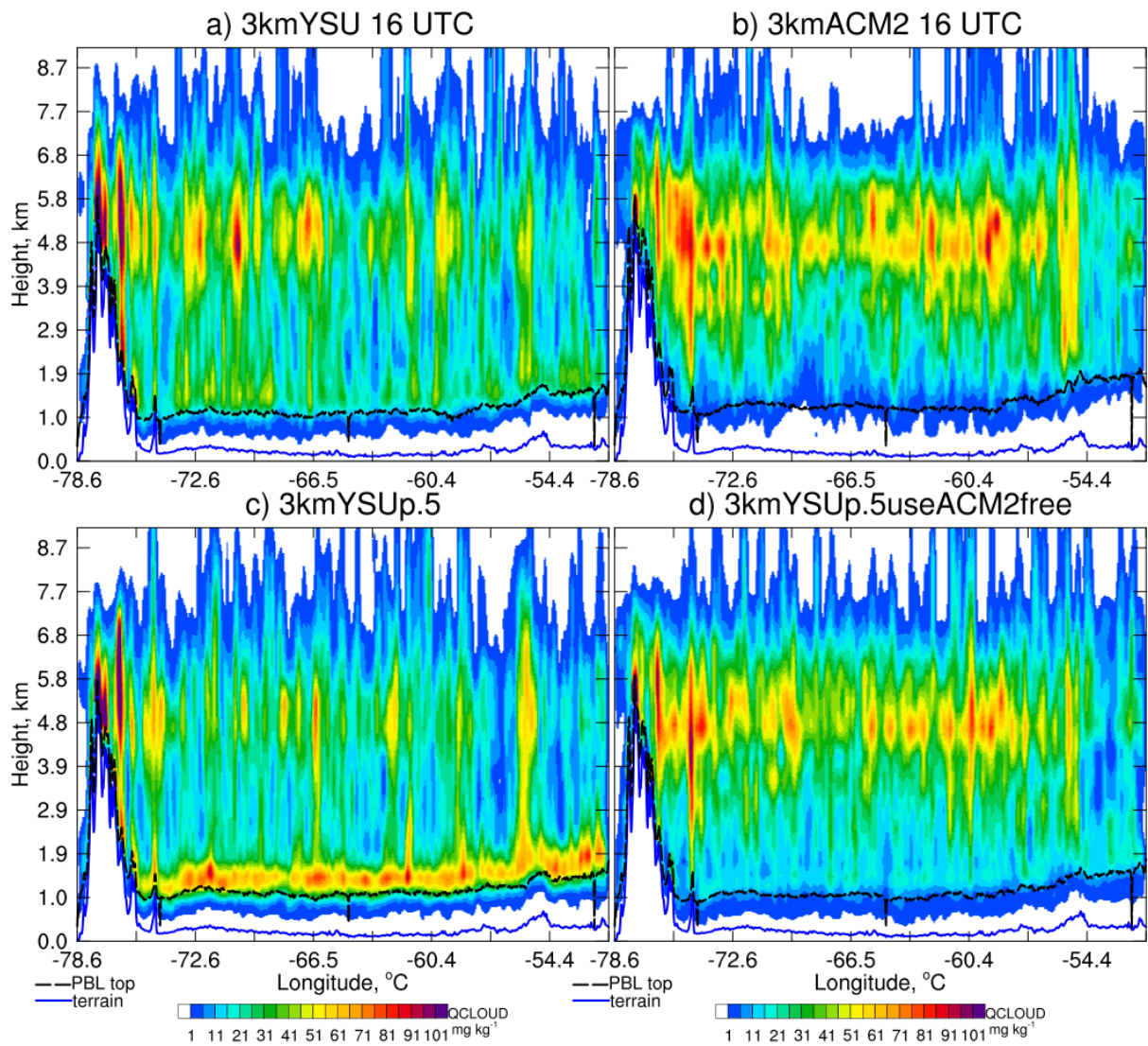
Figure 11. Cross-section of average noon-time cloud water mixing ratios over the Amazon in Jan-Feb 2019 simulated by (a) 3kmYSU , (b) 3kmACM2 , (c) 3kmYSUp.5 , and (d) 3kmYSUp.5useACM2free. The location of these cross-sections is marked in Fig. 4l
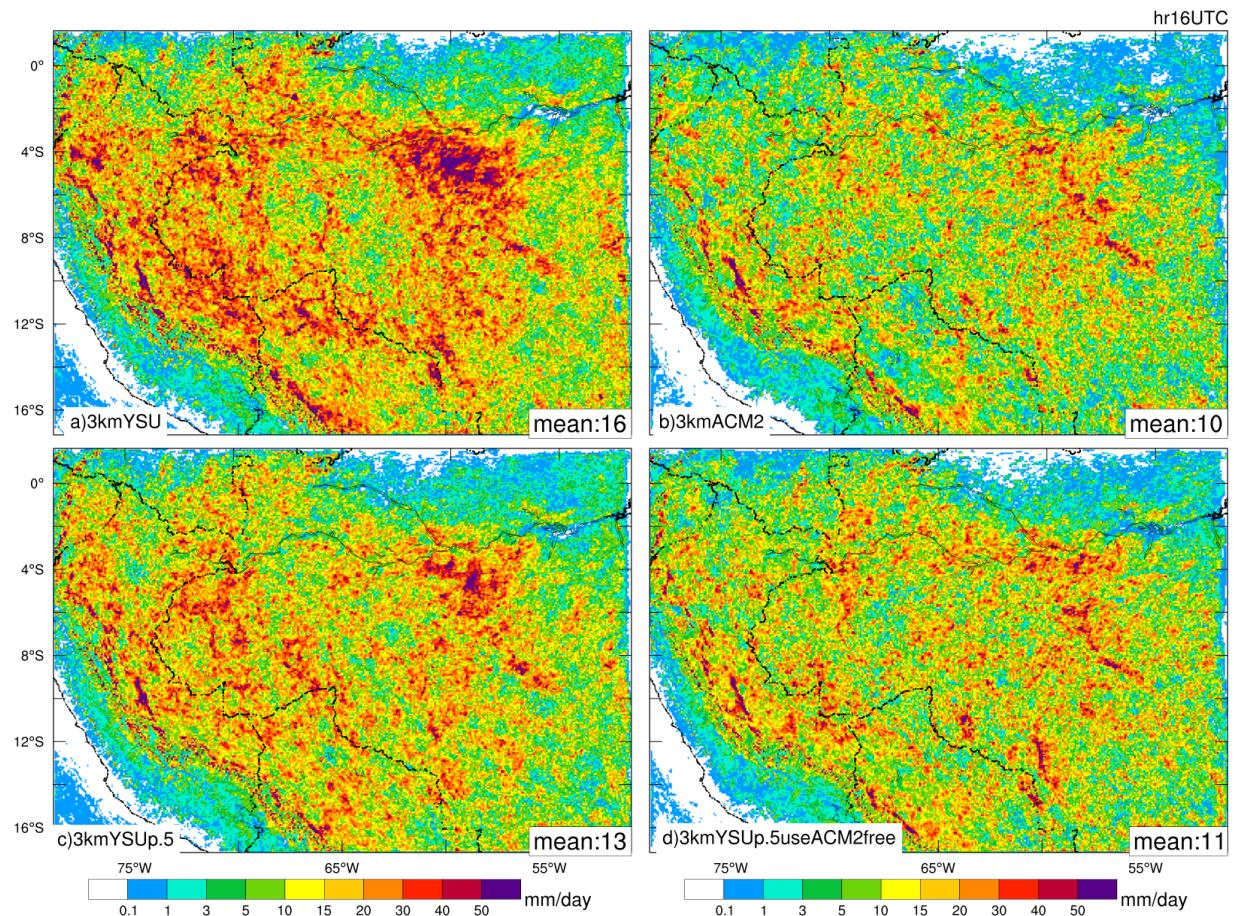
Figure 12. Average noon-time precipitation rate in Jan-Feb 2019 simulated by (a) 3kmYSU, (b) 3kmACM2, (c) 3kmYSUp.5, and (d) 3kmYSUp.5useACM2free. The domain-averaged values are marked.

1 **Effects of lower troposphere vertical mixing on simulated clouds and precipitation over the**
2 **Amazon during the wet season**
3

4 Xiao-Ming Hu[1,2], Yongjie Huang[1], Ming Xue[1,2], Elinor Martin[2], Yang Hong[3], Mengye Chen[3],
5 Hector Mayol Novoa[4], Renee McPherson[5], Andres Perez[4], Isaac Yanqui Morales[4], Auria Julieta
6 Flores Luna[4]
7

8 [1] Center for Analysis and Prediction of Storms, University of Oklahoma, Norman, Oklahoma,
9 73072, USA
10 [2] School of Meteorology, University of Oklahoma, Norman, Oklahoma, 73072, USA
11 [3] School of Civil Engineering and Environmental Engineering, University of Oklahoma,
12 Norman, Oklahoma, 73072, USA
13 [4] Universidad Nacional de San Agustín de Arequipa, Arequipa, Perú
14 [5] Department of Geography and Environmental Sustainability, University of Oklahoma, Norman,
15 Oklahoma, 73072, USA
16

17 Submitted to

18 *Journal of Geophysical Research-Atmospheres*

19 on 1/19/2023 3:47 PM
20

21 Corresponding author address:
22 Drs. Xiao-Ming Hu (xhu@ou.edu), Ming Xue (mxue@ou.edu)
23 Hector Mayol Novoa (hnovoa@unsa.edu.pe),
24 Phone: (405) 325- 0402
25 Center for Analysis and Prediction of Storms, and School of Meteorology
26 University of Oklahoma
27 Norman, Oklahoma 73072, USA
28
29

30 **Key points:** (≤140 characters)
31

32 1. disentangle the turbulence/cloud/precipitation processes over Amazon and reveal root
33   causes for precipitation sensitivity to PBL schemes.

34 2. FT mixing becomes prominent in the presence of clouds, which in turn supports
35   maintenance of the FT clouds that would otherwise dissipate.

36 3. Stronger vertical moisture relay transport in ACM2 PBL scheme supports thicker FT
37   clouds, leading to reduced heating and precipitation.

38
39
40

Abstract

Planetary boundary layer (PBL) schemes parameterize unresolved turbulent mixing within the PBL and free troposphere (FT). Previous studies reported that precipitation simulation over the Amazon in South America is quite sensitive to PBL schemes and the exact relationship between the turbulent mixing and precipitation processes is, however, not disentangled. In this study, regional climate simulations over the Amazon in January-February 2019 are examined at process level to understand the precipitation sensitivity to PBL scheme. The focus is on two PBL schemes, the Yonsei University (YSU) scheme, and the asymmetric convective model v2 (ACM2) scheme, which show the largest difference in the simulated precipitation. During daytime, while the FT clouds simulated by YSU dissipate, clouds simulated by ACM2 maintain because of enhanced moisture supply due to the enhanced vertical moisture relay transport process: 1) vertical mixing within PBL transports surface moisture to the PBL top, and 2) FT mixing feeds the moisture into the FT cloud deck. Due to the thick cloud deck over Amazon simulated by ACM2, surface radiative heating is reduced and consequently the convective available potential energy (CAPE) is reduced. As a result, precipitation is weaker from ACM2. Two key parameters dictating the vertical mixing are identified, p, an exponent determining boundary layer mixing and λ, a scale dictating FT mixing. Sensitivity simulations with altered p, λ, and other treatments within YSU and ACM2 confirm the precipitation sensitivity. The FT mixing in the presence of clouds appears most critical to explain the sensitivity between YSU and ACM2.

Plain Language Summary (≤200 words)

Predictions of weather and climate in terms of clouds and precipitation over the Amazon in South America are quite uncertain. This uncertainty has been largely attributed to errors in the planetary boundary layer (PBL) scheme, which represents turbulent mixing. A lack of understanding of the relationship between turbulence, clouds, and precipitation processes prevents us from improving PBL representation in models to achieve better weather and climate simulations.

This study disentangles the turbulence/clouds/precipitation relationship, and identifies the root cause of model errors in PBL schemes using regional climate simulations over the Amazon. Two PBL schemes, the Yonsei University (YSU) scheme, and the asymmetric convective model v2 (ACM2) scheme, are examined, which show the largest difference in the simulated precipitation.

71   The main difference between the two PBL schemes is the dissipation (YSU) or maintenance
72   (ACM2) of clouds during daytime above the boundary layer, which modulates surface heating and
73   consequently precipitation. The maintenance of a thick cloud deck over the Amazon in ACM2, is
74   caused by enhanced vertical transport of moisture from the surface to above the boundary layer.
75   Such an improved understanding of the turbulence/clouds/precipitation relationship allow us to
76   propose potential solutions to improve PBL schemes in weather and climate models
77
78
79   **Keywords**: Clouds, precipitation, free troposphere vertical mixing, regional climate dynamical
80   downscaling
81
82

1. Introduction

Climate change can cause shifted weather patterns, more extreme weather events, reduced water availability, change in agricultural patterns and increased exposure to disease (Langenbrunner et al., 2019; Prein et al., 2017; Vera et al., 2006) and other significant impacts on society. Accurate simulation of regional climate and the development of adaptation strategies and corresponding policies are critical. Global climate model (GCM) simulations are too coarse to resolve local forcing and local weather, and their precipitation simulation is generally poor. Cloud-resolving regional climate model (RCM) simulations have emerged in recent years for dynamically downscaling global climate simulations and climate change responses at spatial scales that are more useful for decision making (Huang et al., 2022; Liu et al., 2022; Prein et al., 2022; Prein et al., 2015; Prein et al., 2017; Sun et al., 2016). However, compared to mid-latitude regions, the performance of RCM simulations in reproducing precipitation over tropical regions, such as the Amazon in South America, is understudied (Chakraborty et al., 2020; Prein et al., 2022; Tai et al., 2021).

Noontime and afternoon mesoscale convective systems (MCSs) are the main source of precipitation over the Amazon and thus Amazonian precipitation has a single afternoon peak in diurnal cycle (Giangrande et al., 2017; Giangrande et al., 2020; Prein et al., 2022; Wu et al., 2021a). Moist advection from the Atlantic Ocean by northeasterly trade winds during the austral summer wet season (January - February) and zonal wind convergence are important for precipitation over the Amazon rainforest (Fu et al., 1999) and cloud and turbulence processes play critical roles in modulating precipitation in the region (Barber et al., 2022; Chakraborty et al., 2020; Chakraborty et al., 2018; Prein et al., 2022; Wright et al., 2017). The relationship between processes of clouds, turbulence, and precipitation in the region remains to be disentangled and their modelling uncertainties and sensitivities need to be understood to improve simulations (Giangrande et al., 2017; Giangrande et al., 2020; Prein et al., 2022).

Simulated precipitation over the Amazon is sensitive to the planetary boundary layer (PBL) scheme, but the root cause for such sensitivity and the cause-effect relationship remain to be disentangled (Prein et al., 2022). Within typical weather and climate models, PBL schemes parameterize unresolved turbulent mixing within the PBL and the free troposphere; the PBL schemes are therefore critical for reproducing the bulk boundary layer structures and profiles in the whole atmospheric column, as well as their subsequent effects on weather and climate

4

simulations. Many studies (Gunwani & Mohan, 2017; Hu et al., 2012; Hu et al., 2013a; Hu et al., 2010a; Hu et al., 2019; Wang & Hu, 2021) have evaluated the performance of various modern PBL schemes, with most of them focusing on continental cloud-free PBL. Compared to continental clear PBL, much less is known about the performance of PBL schemes in presence of clouds (Angevine et al., 2012; Huang et al., 2013; Supinie et al., 2022; Yang et al., 2019).

PBL schemes can be classified into local and nonlocal schemes. Local schemes estimate the turbulent fluxes at each point in a model from the mean atmospheric variables and/or their gradients at that point, whereas nonlocal schemes include turbulent fluxes based on the atmospheric variables and their variations over a deeper layer covering multiple model levels through the PBL (Cohen et al., 2015; Hu et al., 2010a). The assumption among local schemes that fluxes depend solely on local values and local gradients of model state variables is least valid under convective conditions when turbulent fluxes are dominated by large eddies that transport fluid over longer distances (Hu et al., 2010a). Previous studies found that traditional local schemes (e.g., Mellor–Yamada–Janjić (MYJ) or quasi-normal scale elimination (QNSE)) predict daytime continental boundary layers that are too cool and shallow; while schemes that include non-local treatment, such as the Asymmetrical convective model, version 2 (ACM2, Pleim, 2007), the Yonsei University (YSU, Hong et al., 2006) schemes and the more recently-updated local scheme (e.g., Mellor–Yamada Nakanishi and Niino (MYNN, Nakanishi & Niino, 2006)) predict deeper and warmer daytime continental boundary layers than MYJ and QNSE (Bright & Mullen, 2002; Clark et al., 2015; Coniglio et al., 2013). Also, nonlocal PBL schemes can reproduce the slightly stable upper convective boundary layer while local schemes often fail to do so (Hu et al., 2019; Wang et al., 2016).

Recent PBL development has started to use the mass flux (MF) approach that has been commonly used in cumulus parameterization schemes for large-eddy nonlocal mixing together with the eddy-diffusivity (ED) closure parameterizing local mixing, such as the MYNN-EDMF scheme (Angevine et al., 2010; Olson et al., 2019a; Olson et al., 2019b; Pergaud et al., 2009). Most previous PBL modeling studies focus on treatments within the boundary layer while free-troposphere treatments rarely receive much attention (Hu et al., 2012; Lu & Wang, 2019; Zhu et al., 2021; Zhu et al., 2019), likely because that free-troposphere turbulence is weak under clear conditions and the impact of its parameterization on weather and climate simulations is regarded as minor.

144   Huang et al. (2022) conducted nested-domain RCM simulations with grid spacings of 15

145   and 3 km over the Amazon with different physics schemes. It is found that the simulated

146   precipitation is most sensitive to PBL schemes with the YSU scheme significantly overpredicting

147   Amazonian precipitation and the ACM2 scheme predicting the weakest precipitation. Extending

148   the work of Huang et al. (2022), this study aims to understand the precipitation sensitivity over the

149   Amazon at a process level and identify the root cause for the different model behaviors, with

150   particular attention paid to the behaviors and effects of PBL schemes in cloudy environments, and

151   both inside and above the PBL. Effects of lower troposphere vertical mixing on simulated clouds

152   and precipitation over the Amazon will be elucidated.

153   The rest of this paper is organized as follows: In section 2, precipitation data, model

154   configurations, and numerical experiment design are described. In section 3, clouds/precipitation

155   sensitivity to PBL schemes is diagnosed using simulations with YSU and ACM2 and their variants

156   with altered turbulence treatments, followed by discussion of such sensitivity at a finer resolution.

157   Meanwhile the turbulence/cloud/precipitation processes over the Amazon are examined. Finally,

158   section 4 contains a summary and discussion of the main findings.

159

160   **2. Precipitation data, model configuration and numerical experiment design**

161   a)   Precipitation data

162   Two gridded global precipitation datasets are used in this study to compare with

163   simulations, including (1) half-hourly Integrated Multi-satellitE Retrievals for GPM (IMERG) at

164   a horizontal resolution of 0.1° × 0.1° (Huffman et al., 2019), and (2) half-hourly National Oceanic

165   and Atmospheric Administration (NOAA) Climate Prediction Center (CPC) MORPHing

166   Technique (CMORPH) global precipitation analyses at a horizontal resolution of ∼8 km (Joyce et

167   al., 2004).

168

169   b)   Model configurations

170   Huang et al. (2022) used the Weather Research and Forecasting (WRF) model Version

171   4.2.1 (Skamarock & Klemp, 2008; Skamarock et al., 2021) to perform historical simulations over

172   South America during January-February 2019 in preparation for future regional climate dynamic

173   downscaling. The simulations used hourly European Centre for Medium-Range Weather Forecasts

174   Reanalysis v5 (ERA5, Hersbach et al., 2020) for initial and boundary conditions. Two one-way

175   nested domains with 15- and 3-km horizontal grid spacings cover the entire South America and
176   the Peruvian central Andes region, respectively (see Fig. 1a for domain coverage). Both domains
177   use 61 stretched vertical levels topped at 20 hPa. Following previous dynamic downscaling
178   practices (Hu et al., 2018; Miguez-Macho et al., 2004, 2005; Wang & Kotamarthi, 2013), spectral
179   nudging technique is applied to the outer 15-km domain to maintain large-scale circulations at a
180   1500 km scale, while allowing WRF to evolve smaller-scale dynamics and physics. Twelve
181   sensitivity experiments were conducted by Huang et al. (2022) with varied PBL, microphysics
182   schemes, and land surface models while other physics parameterizations were kept the same
183   among the sensitivity experiments, including revised MM5 Monin-Obukhov surface layer scheme
184   (Jiménez et al., 2012), and the Rapid Radiative Transfer Model for GCMs (RRTMG) longwave
185   and shortwave radiation scheme (Iacono et al., 2008). The Tiedtke cumulus parameterization
186   scheme (Tiedtke, 1989) is used on the 15-km outer domain but not on the 3-km inner domain.

187   These WRF downscaling simulations are found to be most sensitive to PBL schemes with
188   the YSU scheme significantly overpredicting Amazonian precipitation, the ACM2 scheme
189   predicting the weakest precipitation, and the MYNN-EDMF prediction being in the middle. Such
190   relative differences are maintained with altered microphysics schemes and land surface models
191   (LSMs). Simulations with the Thompson microphysics scheme (Thompson et al., 2008), and the
192   Noah LSM (Chen & Zhang, 2009) are chosen to investigate PBL sensitivities in this study.
193   Diagnosing the root cause for the differences between the YSU and ACM2 PBL schemes and
194   disentangle the impact of PBL schemes on precipitation are the foci of this study. Since simulated
195   precipitation is quite sensitive to some other parameterization, such as cumulus schemes (Hu et al.,
196   2018), and there are large uncertainties among different precipitation data (Chen et al., 2022),
197   recommending an optimal PBL scheme in terms of reproducing precipitation is beyond the scope
198   of this study, which may require more advanced profile measurements (e.g., cloud water profile)
199   and more accurate precipitation data to justify as will be seen in our later analyses.

200

201   c) Sensitivity simulations with altered treatments in ACM2 and YSU

202   In addition to the simulations conducted by Huang et al. (2022), eight more sensitivity
203   simulations (summarized in Table 1) are run to help identify the root cause of the differences
204   between ACM2 and YSU, and resolution dependence of the differences, as well as to examine
205   impact of turbulent processes on cloud and precipitation processes. ACM2 and YSU differ in their

206   treatments in both PBL and free troposphere. Sensitivity simulations adjusting either PBL or free-

207   troposphere mixing treatments or both are conducted.

208   In the PBL, while a counter-gradient term is added to the eddy diffusion equation to handle

209   nonlocal mixing in YSU, ACM2 explicitly simulates the transilient nonlocal mass flux. For the

210   local mixing in the PBL, both ACM2 and YSU use a polynomial function/profile (so called K-

211   profile, Noh et al., 2003) to define the vertical mixing coefficient K_z as:

212 $$K_z = k \frac{u_*}{\emptyset} z (1 - \frac{z}{h})^p \qquad (1)$$

213   where k is the von Karman constant, ϕ is the similarity profile function, z is the height above ground

214   level, and h is the PBL height. Thus, ACM2 and YSU are also categorized into the K-profile PBL

215   schemes (Hu et al., 2019). In YSU and ACM2, the value of the exponent p in (1) is 2, but it may

216   vary from 0.5 to 3 depending on flow conditions, with a larger/smaller p yielding smaller/larger

217   K_z (Hu et al., 2018; Hu et al., 2010b; Nielsen-Gammon et al., 2010; Troen & Mahrt, 1986). While

218   a similar local mixing treatment is adopted in ACM2 and YSU, there are many differences in their

219   parameter values, profile functions, methods to diagnose PBL height, etc. ACM2 generally

220   simulates stronger vertical mixing in the PBL and higher PBL height under clear conditions (Hu

221   et al., 2010a). Since p effectively dictates the vertical mixing within the PBL, p is varied in

222   sensitivity simulations to understand model differences and physics processes including turbulence,

223   clouds, and precipitation.

224   In the free troposphere, both YSU and ACM2 compute the K_z as a function of mixing

225   length l, vertical wind shear S, and the stability function $f(Ri)$:

226 $$K_z = l^2 S f(Ri) , \qquad (2)$$

227   in which

228 $$\frac{1}{l} = \frac{1}{kz} + \frac{1}{\lambda} , \qquad (3)$$

229   where Ri is the Richardson number, and λ is the asymptotic length scale. Such first-order

230   parameterizations of turbulent vertical mixing are widely used in operational numerical weather

231   prediction (NWP) and climate models (Beare et al., 2006; Cuxart et al., 2006). ACM2 and YSU

232   differ in their parameter values, Ri calculation within clouds, and stability functions. Both ACM2

233 and YSU use moist-air *Ri* calculation adapted from Durran and Klemp (1982), but YSU requires

234 two layers of clouds to activate the moist-air *Ri* calculation between the two layers while ACM2

235 only requires one layer, in addition to other differences in parameters. Much of the improvement

236 to such parameterizations (Eqs. 2-3) in NWP and climate models involved adjusting the stability

237 functions (for example short vs. long-tailed functions) and λ (Cuxart et al., 2006). λ is adjustable

238 and varies between 30 and 250 m in numerical models (Cuxart et al., 2006; Liu & Carroll, 1996;

239 Nielsen-Gammon et al., 2010). λ is set to 30 m in the YSU scheme and to 80 m in the ACM2

240 scheme. Sensitivity simulations are conducted in this study by replacing the whole free-

241 troposphere treatments or only altering the value of λ.

242 The sensitivity simulations are conducted with the outer 15 km domain because the

243 difference between inner-domain outputs from our nested-domain runs with different

244 configurations are rooted from the different simulations in the outer 15km domain, as we will see

245 in our analysis. Thus, the conclusions from these sensitivity simulations have implications for

246 regional and global models that run at convection-parameterized resolutions. In addition, four

247 sensitivity simulations with a single domain covering the majority of the Amazon with a 3 km grid

248 spacing are also conducted to examine the applicability of conclusions obtained at 15 km grid

249 spacing to convection-allowing simulations.

250

3. Results

252 a) Cause of precipitation differences simulated with different PBL schemes

253 As stated earlier, WRF simulations over South America during January-February 2019 are

254 conducted with 12 different physics schemes, including PBL, microphysics schemes and land

255 surface models (Huang et al., 2022). The simulated precipitation is most sensitive to PBL schemes

256 (Huang et al., 2022) with the YSU scheme predicting the strongest daily precipitation rate while

257 the ACM2 scheme predicting the weakest precipitation over the Amazon during the summer wet

258 season (Fig. 1). The relative strength of simulated precipitation between ACM2 and YSU remains

259 across different resolutions, including the convection-parameterized (15 km grid spacing) and

260 convection-permitting (3 km grid spacing) resolutions. The precipitation rate increases with

261 increased resolution. The YSU runs at 3 km grid spacing (including the nested run focusing on

262 Peru and the single-domain run focusing more on the Amazon) significantly overestimate daily

263   precipitation rate (Figs. 1c-f). The South America Affinity Group (SAAG) led by National Center

264   for Atmospheric Research (NCAR) also reported that a WRF simulation using the YSU scheme at

265   a grid spacing of 4 km over South America overestimated precipitation over the Amazon (Liu et

266   al., 2022).

267   Precipitation over the Amazon is dominated by mid-day and afternoon MCSs (Giangrande

268   et al., 2017; Giangrande et al., 2020; Prein et al., 2022; Wu et al., 2021a). Thus, we will focus on

269   the precipitation and related processes during daytime. During mid-day hours, YSU simulates

270   stronger hourly precipitation rates than ACM2 and overestimates precipitation at both resolutions

271   and over different domains (Fig. 2).

272   Causative factors for the different precipitation simulated by ACM2 and YSU over the

273   Amazon are herein investigated. The impact of different PBL schemes on NWP and climate

274   simulations is more straightforward under clear conditions while their impacts on precipitation is

275   less clear. Often the impact of PBL schemes on precipitation is not conclusive because the

276   schemes produce different (stronger or weaker) precipitation in different cases (Bright & Mullen,

277   2002; Cohen et al., 2015; Jankov et al., 2005; Jankov et al., 2007; Li & Pu, 2008; Supinie et al.,

278   2022; Wu et al., 2021b; Zhang et al., 2013). Under clear conditions, ACM2 simulates stronger

279   boundary layer vertical mixing and deeper PBL than YSU due to different treatments for nonlocal

280   fluxes and different parameters/functions in the K-profile local mixing (Hu et al., 2010a; Nielsen-

281   Gammon et al., 2010; Shin & Hong, 2011; Xie et al., 2012). How such differences translate to

282   significantly different precipitation with the two schemes is the main question to be answered in

283   this study.

284   Surface temperature shows distinct differences over the Amazon with the ACM2

285   simulating lower continental temperatures than YSU by 0.5-0.8 °C over the simulation domains

286   around noon (Fig. 3), which likely leads to less surface energy to feed MCSs. The lower

287   temperature simulated by ACM2 covers the main precipitation region over the Amazon (Fig. 3g)

288   and can likely explain the precipitation difference. However, such temperature differences cannot

289   be explained by the direct impact of PBL mixing. Prior work has shown that during daytime,

290   ACM2 simulates stronger mixing in the PBL and stronger PBL-free troposphere exchange

291   generally warming up the PBL due to entrainment of free troposphere air with higher potential

292   temperature (Hu et al., 2010a; Shin & Hong, 2011). Thus, the direct impact of ACM2 PBL mixing

293   should lead to higher surface temperature, rather than the lower temperature obtained in the regions

294   of precipitation.

295   Rather, the temperature difference between ACM2 and YSU simulations is more directly

296   related to the difference in surface downward shortwave radiation. ACM2 simulates less

297   shortwave radiation at the surface over the Amazon region (Fig. 4g), where cloud coverage is

298   significant (Fig. 4j). At 17 UTC (12-14 LST across south America), the average surface shortwave

299   radiation simulated by ACM2 is lower by ~70 W m^{-2} than the YSU runs. Thus, the lower

300   temperature simulated by ACM2 should be due to indirect effects of vertical mixing via

301   interactions with clouds and radiation.

302   Significant cloud coverage over the Amazon (Kay et al., 2016; Kay et al., 2012) is a

303   characteristic distinguishing this study from most other studies of PBL schemes. Over the

304   Amazonian region, ACM2 simulates a thicker cloud deck (Fig. 5,6), which reduces downward

305   shortwave radiation (Fig. 7), consequently leading to a lower surface temperature. As a result, the

306   surface-based convective available potential energy (CAPE) is lower in the ACM2 simulations

307   (Fig. 8), which would lead to weaker daytime precipitation. The significant difference between

308   YSU and ACM2 is mostly confined over the cloud region (Fig. 4 & 7), which further confirms

309   that indirect effects of vertical mixing over the Amazon via interactions with clouds dominates its

310   direct effects.

311   The cloud deck over the Amazon therefore appears to be a critical link to disentangle the

312   impact of PBL schemes on simulated precipitation. During daytime, while the clouds simulated

313   with the YSU scheme dissipate gradually from the early morning maxima, clouds simulated with

314   the ACM2 scheme are still sustained through the day (see cloud cross-sections at 11 - 21 UTC in

315   Fig. 5). Daytime cloud thinning is likely due to solar heating under condition of lack of water

316   vapor supply available for condensation (Adebiyi et al., 2020; Burleyson & Yuter, 2015; Painemal

317   et al., 2015; Zhang et al., 2010). The thicker cloud deck simulated by ACM2 appears to be due to

318   enhanced supply of boundary layer moisture to the layers above (thus less boundary layer moisture

319   by 0.6 g kg^{-1} and more free troposphere moisture by 0.2 g kg^{-1} compared to the YSU run, Fig. 9b),

320   through enhanced boundary layer vertical mixing (Hu et al., 2010a; Shin & Hong, 2011).

321   In the nested-domain simulations, surface temperature simulated by ACM2 is lower than

322   YSU in both 15 and 3 km domains (Fig. 3) and the resulting lower precipitation occurs in both

323   domains. The root cause of lower surface temperatures from ACM2 in the nested 3 km domain is

324   less clear due to the possible effect of 15 km simulations (such as advection) through its lateral

325   boundaries. Thus, the main discussions below (in section b) will focus on further investigation of

326   PBL-clouds-precipitation relationship in the outer 15 km domain with additional simulations with

327   altered treatments, while their relationship at the convection-permitting resolution will be

328   examined with additional single-domain simulations with a 3 km grid spacing (in section c).

329

330   b) Impact of different turbulence treatments on clouds and precipitation

331   Lower troposphere turbulence plays important roles in cloud production and maintenance

332   (Lilly, 1968). This section discusses results of sensitivity simulations adjusting turbulence

333   treatments in YSU and ACM2. Since under clear conditions, ACM2 has stronger daytime

334   boundary layer mixing than YSU (Hu et al., 2010a; Shin & Hong, 2011), vertical mixing in the

335   YSU PBL scheme is first enhanced to see if the simulated clouds and precipitation would become

336   closer to those simulated by ACM2. The exponent p in the K-profile in YSU (default value is 2)

337   is reduced to 0.5 in experiment YSUp.5 to enhance daytime boundary layer mixing, as indicated by

338   the K_z profiles in Fig. 9d. With $p=0.5$, YSUp.5 simulates higher PBL top height (Fig. 9d). As a

339   result, more near-surface moisture is transported to the top of the elevated PBL, where a thicker

340   cloud layer near the PBL top forms (Fig. 6c & Fig. 9c). Note that while the nonlocal mixing is

341   proportional to K_z in YSU, transilient nonlocal fluxes are explicitly simulated by ACM2, which is

342   not shown in Fig. 9. Thus K_z profiles in Fig. 9d are more indicative of total mixing in the boundary

343   layer for YSU, but less so for ACM2. In the free troposphere where there are no nonlocal mixing

344   treatments for either scheme, thus K_z profiles are indicative of free-troposphere mixing for both.

345   As the PBL grows in the daytime, the PBL top clouds simulated by both YSU and ACM2

346   keep elevating (Fig. 5). A more prominent/distinct PBL top cloud layer is simulated by YSU (Fig.

347   5c,e, PBL top is marked by black dash lines) while the PBL top clouds simulated by ACM2 are

348   indistinctive from the free-troposphere clouds (Fig. 5d,f). Existence of a PBL top cloud layer over

349   the Amazon was previously illustrated by cloud frequency data observed during the GoAmazon

350   2014/5 field experiments (Giangrande et al., 2017; Giangrande et al., 2020). However, that dataset

351   only provides cloud frequency, not cloud amount. To quantitatively verify the simulated PBL top

352   cloud layer, more advanced cloud dataset is needed.

353   The thickened PBL top clouds simulated by YSU with $p=0.5$ weakens surface shortwave

354   radiation (Fig. 7) and consequently lowers surface temperature and CAPE (Fig. 8), thus reduces

12

355 precipitation (Fig. 10). Such a precipitation sensitivity to boundary layer mixing over the Amazon

356 is consistent with that reported over the eastern United States (Hu et al., 2018). However, YSU

357 with p=0.5 does not reduce precipitation to the level simulated by ACM2 (Fig. 10). In comparison,

358 ACM2 simulates a more prominent cloud layer at a higher elevation (~4-5 km above ground) while

359 the clouds simulated by YSU at this altitude (with both default p value and p=0.5) weaken in time

360 during the day (Fig. 5). Thus, boundary layer mixing alone cannot completely explain the different

361 impacts of ACM2 and YSU on clouds.

362   In addition to the different treatments within the boundary layer, ACM2 and YSU also

363 differ in their treatments in the free troposphere. A YSU sensitivity simulation using ACM2's

364 free-troposphere mixing treatment (named YSUuseACM2free) is conducted to examine the impact

365 of free troposphere mixing. YSUuseACM2free simulates a stronger vertical mixing up to 7-8 km

366 above the ground, particularly in presence of clouds, similar to the ACM2 simulation (Fig. 9d).

367 Further up, the sensitivity of vertical mixing is small and K_z is simulated to be less than 0.1 m^2 s^{-1}

368 by all schemes. Thus, our analysis focuses on the lower free troposphere. As a result of stronger

369 mixing in the lower free troposphere, a thicker cloud deck at 4-5 km above ground (Fig. 6d), similar

370 to ACM2 (Fig. 6b), develops in the simulation, likely due to stronger moisture supply from the

371 PBL top. Consequently, surface temperature is reduced due to cloud shield, and the precipitation

372 is reduced, to be closer to that of ACM2 than YSUp.5 (Fig. 10). Combining both p=0.5 and

373 ACM2's free-troposphere mixing, YSUp.5useACM2free simulates a similar, but slightly thicker

374 cloud deck (Fig. 6e) and slightly weaker precipitation than YSUuseACM2free (Fig. 10). These

375 experiments illustrate that free-troposphere mixing is the most critical difference between YSU

376 and ACM2 in terms of simulating clouds and precipitation, while the mixing in the PBL plays a

377 secondary role.

378   For free troposphere vertical mixing, ACM2 and YSU differ in their parameters, moist-air

379 Ri calculation, and the stability functions. Previous studies identified λ as a critical parameter for

380 free-troposphere mixing (Cuxart et al., 2006; Hu et al., 2012; Nielsen-Gammon et al., 2010), and

381 here its impact is further examined. An ACM2 sensitivity simulation with λ=30 (named

382 ACM2λ30) is conducted to verify its impact on clouds/precipitation. Comparing to default ACM2

383 with λ=80, ACM2λ30 simulates a much weaker mixing in the free troposphere (Fig. 9d), and

384 consequently a much thinner cloud deck at 4-5 km above ground and meanwhile the PBL top

385 clouds appear thicker (Fig. 6f), likely due to weaker vertical transport of moisture from the PBL

386   top to higher levels. The net result is that the surface radiation is enhanced (Fig. 7f), temperature
387   is higher, and more precipitation is produced (Fig. 10f). The precipitation simulated by
388   ACM2λ30 is not as strong as that simulated by YSU because of other differences in free-
389   troposphere and PBL mixing treatments.

390   All the above results together suggest a prominent *PBL-free-troposphere moisture relay*
391   *transport process*: Step 1, boundary layer mixing transports moisture to the PBL top where clouds
392   form; step 2, free-troposphere mixing transports the moisture further to higher levels ($\sim$ 4-5 km)
393   to sustain a thick cloud deck at that altitude and reduce the boundary layer top clouds
394   somewhat. *ACM2 simulates a strong PBL-free-troposphere moisture relay transport process.*
395   Comparing to YSU, ACM2 simulates less PBL moisture (by 0.5 g kg^{-1}) and more free troposphere
396   moisture (by 0.2 g kg^{-1} at 3-6.5 km above ground, Fig. 9b) in monthly average. Consequently, the
397   free-troposphere cloud layer is better maintained during daytime. In contrast, the moisture relay
398   transport process simulated by YSU is weaker and the clouds at $\sim$ 4-5 km dissipate quicker during
399   daytime, leading to less cloud coverage, more CAPE and precipitation. Modified YSU with
400   enhanced PBL and free-troposphere mixing (YSUp.5useACM2free) produces similar moisture
401   transport as ACM2 (Fig. 9b,d) hence reduced precipitation. These results suggest that free-
402   troposphere mixing may become prominent in the presence of clouds (which otherwise would be
403   weak as generally regarded) and become an important step in the relay transport process. To verify
404   the strength of such relay transport process, more advanced observations, such as long-term
405   vertical profiles of cloud mixing ratios, are warranted. Our results also suggest that to correctly
406   simulate clouds/precipitation in environments similar to those of the Amazon, the ability of models
407   in reproducing such moisture relay transport processes needs to be carefully assessed.

408
409   *c)* Sensitivity of clouds and precipitation to different turbulence treatments at a convection-
410   allowing resolution

411
412   The sensitivity of simulated clouds and precipitation to boundary layer and free-
413   atmosphere vertical mixing discussed above is mainly based on simulations at 15 km grid spacing
414   where cumulus parameterization is employed. Thus, the conclusions are directly applicable to
415   global and regional weather and climate simulations/predictions at convection-parameterized
416   resolutions. Whether these conclusions are still valid at convection-permitting resolutions requires
417   additional examination. To avoid the possible effects of the driving 15 km grid on the nested 3

418 km grid, single-domain sensitivity simulations are conducted that cover a majority of the Amazon
419 with a 3 km grid spacing that use ERA5 data directly as lateral boundary conditions. These
420 simulations include $3kmYSU$, $3kmYSUp.5$, $3kmYSUp.5useACM2free$, and $3kmACM2$ (as
421 summarized in Table 1). Even though simulated precipitation rate is generally higher at the 3 km
422 grid spacing than at 15 km grid spacing, the same turbulent mixing → clouds → precipitation
423 impact/sensitivity holds in these convection-permitting simulations (Fig. 11, 12). That is, 1) YSU
424 simulates stronger daytime precipitation rate than ACM2 (by 60% at noon time, 16 vs. 10 mm day^{-1}
425 , Fig. 12a,b); 2) Stronger boundary layer mixing simulated by YSU with p=0.5 leads to more PBL
426 top clouds (Fig. 11c), which block more shortwave radiation and reduce daytime surface
427 temperature and consequently precipitation (with 13 mm day^{-1} at noon, Fig. 12c); 3) Using the
428 free-troposphere mixing treatment of ACM2 in YSU simulates a more prominent cloud layer at 4-
429 5 km above ground (Fig. 11d) which more effectively blocks shortwave radiation and reduces
430 precipitation (with 11 mm day^{-1} at noon, Fig. 12d) that is closer to the precipitation rate of ACM2
431 (Fig. 12b).
432

433 **4. Conclusions and discussion**
434   Previous studies by others and a recent study of ours found that precipitation simulations
435 over the Amazon in South America are very sensitive to the PBL scheme used. The exact
436 relationship between the turbulent mixing and precipitation processes in that humid region is,
437 however, not clear. In this study, two-month-long simulations over South America in January-
438 February 2019 are examined to understand the precipitation sensitivity to treatments of turbulent
439 mixing in both the PBL and free troposphere within PBL schemes. Two PBL schemes, the YSU
440 and ACM2 schemes, are the foci of this study since they produced the most and least amount of
441 precipitation among PBL schemes examined. Our results serve to disentangle the turbulence –
442 cloud - precipitation processes over the Amazon and reveal root causes for the sensitivity to PBL
443 schemes, which is a prerequisite for future model improvement. During daytime, while the free-
444 troposphere clouds simulated by YSU dissipate due to solar heating, clouds simulated by ACM2
445 maintains through the day because of enhanced moisture supply due to enhanced *PBL-free-*
446 *troposphere* relay transport process: step 1, enhanced vertical mixing within PBL simulated by
447 ACM2 transports surface moisture to the PBL top where clouds first form, and step 2, enhanced
448 free-troposphere mixing feeds the moisture into the free-troposphere cloud deck. Due to the

15

449   thicker cloud deck over the Amazon simulated by ACM2, surface radiative heating is reduced and

450   consequently CAPE is reduced. As a result, precipitation is weaker from ACM2. In contrast, the

451   moisture *PBL-free-troposphere* relay transport process simulated by YSU is weaker and the clouds

452   at ~4-5 km dissipate quicker, and CAPE is therefore larger during daytime, leading to more

453   precipitation. To verify the strength of such relay transport process, more advanced observations

454   are warranted, for example, of long-term vertical profiles of cloud mixing ratios. To correctly

455   simulate clouds and precipitation, model performance of reproducing such a moisture relay

456   transport process needs to be carefully evaluated.

457   Two key parameters dictating the vertical mixing in the YSU and ACM2 schemes are

458   identified, which are p, an exponent in the polynomial function determining boundary layer

459   vertical mixing and λ, the asymptotic length scale dictating free-troposphere mixing. Sensitivity

460   simulations with altered p, λ, and other treatments within YSU and ACM2 confirm the sensitivity

461   of precipitation to the mixing strength. The free-troposphere mixing in presence of clouds become

462   prominent (which is otherwise weak) because of reduced moist static stability and the difference

463   in free-troposphere mixing appears to explain more of the sensitivity to the YSU and ACM2 PBL

464   schemes. The turbulent mixing and cloud relationship over the Amazon simulated with ACM2

465   suggests strong positive feedback through which regions of lower troposphere clouds create

466   conditions favorable for daytime cloud maintenance. Such feedback is weaker with YSU, which

467   leads to daytime breakup of free-troposphere clouds.

468   The above results regarding the turbulence-clouds-precipitation processes and their

469   parameterizations have important implications to the understanding and accurate prediction of

470   weather, climate, as well as air quality over the Amazon region that is humid, cloudy and rich in

471   precipitation. South America is experiencing an increasing trend in summer precipitation, and

472   such a trend is also projected by climate models (Vera et al., 2006). Given the negative cloud-

473   precipitation correlation seen in this study for the Amazon region, such a precipitation trend may

474   imply a decreasing trend of cloud cover in the region. Correct representation of turbulence mixing-

475   cloud-radiation interactions within weather and climate models is clearly critical for accurate

476   simulation/prediction of precipitation and water cycles.

477   Though not shown here, since simulated precipitation is weaker with ACM2, the

478   corresponding tropospheric upward motion is also weaker , so stronger easterly winds impinge on

479   the east side of Andes and are diverted southward to form a stronger southward LLJ east of Andes.

Thus, the simulated strength of Amazonian precipitation is closely linked to the strength of LLJ east of Andes, which may have implications for the simulation of downstream atmospheric environments including temperature and humidity conditions and air quality (Hu et al., 2013b; Hu et al., 2013c; Klein et al., 2014). These are topics for future studies.

Data Availability Statement.

The ERA5 reanalysis data are available at https://doi.org/10.5065/BH6N-5N20. GPM IMERG Final Precipitation dataset is available at https://doi.org/10.5067/GPM/IMERGDF/DAY/06 (last access: 12 November 2020). CMORPH dataset is available at https://ftp.cpc.ncep.noaa.gov/precip/CMORPH_V1.0/CRT/8km-30min (last access: 12 November 2020). Figures in this manuscript are produced using the NCAR Command Language (Version 6.6.2) [Software]. (2019). Boulder, Colorado: UCAR/NCAR/CISL/TDD. http://dx.doi.org/10.5065/D6WD3XH5 . Model data produced from this study have been archived at CAPS website https://caps.ou.edu/micronet/Regionalclimate.html

References

Adebiyi, A. A., Zuidema, P., Chang, I., Burton, S. P., & Cairns, B. (2020). Mid-level clouds are frequent above the southeast Atlantic stratocumulus clouds. *Atmos. Chem. Phys., 20*(18), 11025-11043. 10.5194/acp-20-11025-2020

Angevine, W. M., Eddington, L., Durkee, K., Fairall, C., Bianco, L., & Brioude, J. (2012). Meteorological Model Evaluation for CalNex 2010. *Monthly Weather Review, 140*(12), 3885-3906. 10.1175/Mwr-D-12-00042.1

Angevine, W. M., Jiang, H. L., & Mauritsen, T. (2010). Performance of an Eddy Diffusivity-Mass Flux Scheme for Shallow Cumulus Boundary Layers. *Monthly Weather Review, 138*(7), 2895-2912. 10.1175/2010mwr3142.1

Barber, K. A., Burleyson, C. D., Feng, Z., & Hagos, S. M. (2022). The Influence of Shallow Cloud Populations on Transitions to Deep Convection in the Amazon. *Journal of the Atmospheric Sciences, 79*(3), 723-743. 10.1175/jas-d-21-0141.1

Beare, R. J., MacVean, M. K., Holtslag, A. A. M., Cuxart, J., Esau, I., Golaz, J. C., . . . Sullivan, P. (2006). An intercomparison of large-eddy simulations of the stable boundary layer. *Boundary-Layer Meteorology, 118*(2), 247-272. 10.1007/s10546-004-2820-6

Bright, D. R., & Mullen, S. L. (2002). The sensitivity of the numerical simulation of the southwest monsoon boundary layer to the choice of PBL turbulence parameterization in MM5. *Weather and Forecasting, 17*(1), 99-114. Doi 10.1175/1520-0434(2002)017<0099:Tsotns>2.0.Co;2

Burleyson, C. D., & Yuter, S. E. (2015). Patterns of Diurnal Marine Stratocumulus Cloud Fraction Variability. *Journal of Applied Meteorology and Climatology, 54*(4), 847-866. 10.1175/jamc-d-14-0178.1

Chakraborty, S., Jiang, J. H., Su, H., & Fu, R. (2020). Deep Convective Evolution From Shallow Clouds Over the Amazon and Congo Rainforests. *Journal of Geophysical Research: Atmospheres, 125*(1), e2019JD030962. https://doi.org/10.1029/2019JD030962

Chakraborty, S., Schiro, K. A., Fu, R., & Neelin, J. D. (2018). On the role of aerosols, humidity, and vertical wind shear in the transition of shallow-to-deep convection at the Green Ocean Amazon 2014/5 site. *Atmos. Chem. Phys., 18*(15), 11135-11148. 10.5194/acp-18-11135-2018

Chen, F., & Zhang, Y. (2009). On the coupling strength between the land surface and the atmosphere: From viewpoint of surface exchange coefficients. *Geophysical Research Letters, 36*. L10404, 10.1029/2009gl037980

Chen, M., Huang, Y., Li, Z., Larico, A. J. M., Xue, M., Hong, Y., . . . Morales, I. Y. (2022). Cross-Examining Precipitation Products by Rain Gauge, Remote Sensing, and WRF Simulations over a South American Region across the Pacific Coast and Andes. *Atmosphere, 13*(10), 1666.

Clark, A. J., Coniglio, M. C., Coffer, B. E., Thompson, G., Xue, M., & Kong, F. Y. (2015). Sensitivity of 24-h Forecast Dryline Position and Structure to Boundary Layer Parameterizations in Convection-Allowing WRF Model Simulations. *Weather and Forecasting, 30*(3), 613-638. 10.1175/Waf-D-14-00078.1

Cohen, A. E., Cavallo, S. M., Coniglio, M. C., & Brooks, H. E. (2015). A Review of Planetary Boundary Layer Parameterization Schemes and Their Sensitivity in Simulating Southeastern US Cold Season Severe Weather Environments. *Weather and Forecasting, 30*(3), 591-612. 10.1175/Waf-D-14-00105.1

Coniglio, M. C., Correia, J., Marsh, P. T., & Kong, F. Y. (2013). Verification of Convection-Allowing WRF Model Forecasts of the Planetary Boundary Layer Using Sounding Observations. *Weather and Forecasting, 28*(3), 842-862. 10.1175/Waf-D-12-00103.1

Cuxart, J., Holtslag, A. A. M., Beare, R. J., Bazile, E., Beljaars, A., Cheng, A., . . . Xu, K. M. (2006). Single-column model intercomparison for a stably stratified atmospheric boundary layer. *Boundary-Layer Meteorology, 118*(2), 273-303. 10.1007/s10546-005-3780-1

Durran, D. R., & Klemp, J. B. (1982). On the Effects of Moisture on the Brunt-Väisälä Frequency. *Journal of Atmospheric Sciences, 39*(10), 2152-2158. 10.1175/1520-0469(1982)039<2152:Oteomo>2.0.Co;2

Fu, R., Zhu, B., & Dickinson, R. E. (1999). How Do Atmosphere and Land Surface Influence Seasonal Changes of Convection in the Tropical Amazon? *Journal of Climate, 12*(5), 1306-1321. 10.1175/1520-0442(1999)012<1306:Hdaals>2.0.Co;2

Giangrande, S. E., Feng, Z., Jensen, M. P., Comstock, J. M., Johnson, K. L., Toto, T., . . . Martin, S. T. (2017). Cloud characteristics, thermodynamic controls and radiative impacts during the Observations and Modeling of the Green Ocean Amazon (GoAmazon2014/5) experiment. *Atmos. Chem. Phys., 17*(23), 14519-14541. 10.5194/acp-17-14519-2017

Giangrande, S. E., Wang, D., & Mechem, D. B. (2020). Cloud regimes over the Amazon Basin: perspectives from the GoAmazon2014/5 campaign. *Atmos. Chem. Phys., 20*(12), 7489-7507. 10.5194/acp-20-7489-2020

Gunwani, P., & Mohan, M. (2017). Sensitivity of WRF model estimates to various PBL parameterizations in different climatic zones over India. *Atmospheric Research, 194*, 43-65. https://doi.org/10.1016/j.atmosres.2017.04.026

Hersbach, H., Bell, B., Berrisford, P., Hirahara, S., Horányi, A., Muñoz-Sabater, J., . . . Thépaut, J.-N. (2020). The ERA5 global reanalysis. *Quarterly Journal of the Royal Meteorological Society, 146*(730), 1999-2049. https://doi.org/10.1002/qj.3803

Hong, S. Y., Noh, Y., & Dudhia, J. (2006). A new vertical diffusion package with an explicit treatment of entrainment processes. *Monthly Weather Review, 134*(9), 2318-2341. Doi 10.1175/Mwr3199.1

Hu, X.-M., Doughty, D. C., Sanchez, K. J., Joseph, E., & Fuentes, J. D. (2012). Ozone variability in the atmospheric boundary layer in Maryland and its implications for vertical transport model. *Atmospheric Environment, 46*, 354-364. 10.1016/j.atmosenv.2011.09.054

Hu, X.-M., Klein, P. M., & Xue, M. (2013a). Evaluation of the updated YSU planetary boundary layer scheme within WRF for wind resource and air quality assessments. *Journal of Geophysical Research-Atmospheres, 118*(18), 10490-10505. 10.1002/jgrd.50823

Hu, X.-M., Klein, P. M., Xue, M., Lundquist, J. K., Zhang, F., & Qi, Y. (2013b). Impact of Low-Level Jets on the Nocturnal Urban Heat Island Intensity in Oklahoma City. *Journal of Applied Meteorology and Climatology, 52*(8), 1779-1802. 10.1175/jamc-d-12-0256.1

Hu, X.-M., Klein, P. M., Xue, M., Zhang, F., Doughty, D. C., Forkel, R., . . . Fuentes, J. D. (2013c). Impact of the vertical mixing induced by low-level jets on boundary layer ozone concentration. *Atmospheric Environment, 70*, 123-130. 10.1016/j.atmosenv.2012.12.046

Hu, X.-M., Nielsen-Gammon, J. W., & Zhang, F. Q. (2010a). Evaluation of Three Planetary Boundary Layer Schemes in the WRF Model. *Journal of Applied Meteorology and Climatology, 49*(9), 1831-1844. 10.1175/2010jamc2432.1

Hu, X.-M., Xue, M., & Li, X. (2019). The Use of High-Resolution Sounding Data to Evaluate and Optimize Nonlocal PBL Schemes for Simulating the Slightly Stable Upper

601   Convective Boundary Layer. *Monthly Weather Review, 147*(10), 3825-3841.
602   10.1175/mwr-d-19-0085.1
603 Hu, X.-M., Xue, M., McPherson, R. A., Martin, E., Rosendahl, D. H., & Qiao, L. (2018).
604   Precipitation Dynamical Downscaling Over the Great Plains. *Journal of Advances in*
605   *Modeling Earth Systems, 10*(2), 421-447. 10.1002/2017ms001154
606 Hu, X.-M., Zhang, F., & Nielsen-Gammon, J. W. (2010b). Ensemble-based simultaneous state
607   and parameter estimation for treatment of mesoscale model error: A real-data study.
608   *Geophysical Research Letters, 37*. L08802, 10.1029/2010gl043017
609 Huang, H. Y., Hall, A., & Teixeira, J. (2013). Evaluation of the WRF PBL Parameterizations for
610   Marine Boundary Layer Clouds: Cumulus and Stratocumulus. *Monthly Weather Review,*
611   *141*(7), 2265-2271. 10.1175/Mwr-D-12-00292.1
612 Huang, Y., Xue, M., Hu, X.-M., Martin, E. R., Novoa, H., McPherson, R. A., . . . Morales, I. Y.
613   (2022). *Characteristics of Precipitation and MCS over the Peruvian Central Andes based*
614   *on Convection-Permitting Simulations.* Paper presented at the AGU fall meeting,
615   Chicago, IL, https://agu.confex.com/agu/fm22/meetingapp.cgi/Person/177979.
616 Huffman, G. J., E.F. Stocker, D.T. Bolvin, Nelkin, E. J., & Tan, J. (2019). GPM IMERG Final
617   Precipitation L3 1 day 0.1 degree x 0.1 degree V06 (Publication no.
618   https://doi.org/10.5067/GPM/IMERGDF/DAY/06). Retrieved Nov. 2022
619 Iacono, M. J., Delamere, J. S., Mlawer, E. J., Shephard, M. W., Clough, S. A., & Collins, W. D.
620   (2008). Radiative forcing by long-lived greenhouse gases: Calculations with the AER
621   radiative transfer models. *Journal of Geophysical Research: Atmospheres, 113*(D13).
622   https://doi.org/10.1029/2008JD009944
623 Jankov, I., Gallus, W. A., Segal, M., Shaw, B., & Koch, S. E. (2005). The impact of different
624   WRF model physical parameterizations and their interactions on warm season MCS
625   rainfall. *Weather and Forecasting, 20*(6), 1048-1060. Doi 10.1175/Waf888.1
626 Jankov, I., Schultz, P. J., Anderson, C. J., & Koch, S. E. (2007). The Impact of Different
627   Physical Parameterizations and Their Interactions on Cold Season QPF in the American
628   River Basin. *Journal of Hydrometeorology, 8*(5), 1141-1151. 10.1175/jhm630.1
629 Jiménez, P. A., Dudhia, J., González-Rouco, J. F., Navarro, J., Montávez, J. P., & García-
630   Bustamante, E. (2012). A Revised Scheme for the WRF Surface Layer Formulation.
631   *Monthly Weather Review, 140*(3), 898-918. 10.1175/mwr-d-11-00056.1
632 Joyce, R. J., Janowiak, J. E., Arkin, P. A., & Xie, P. (2004). CMORPH: A Method that Produces
633   Global Precipitation Estimates from Passive Microwave and Infrared Data at High
634   Spatial and Temporal Resolution. *Journal of Hydrometeorology, 5*(3), 487-503.
635   10.1175/1525-7541(2004)005<0487:Camtpg>2.0.Co;2
636 Kay, J. E., Bourdages, L., Miller, N. B., Morrison, A., Yettella, V., Chepfer, H., & Eaton, B.
637   (2016). Evaluating and improving cloud phase in the Community Atmosphere Model
638   version 5 using spaceborne lidar observations. *Journal of Geophysical Research:*
639   *Atmospheres, 121*(8), 4162-4176. https://doi.org/10.1002/2015JD024699
640 Kay, J. E., Hillman, B. R., Klein, S. A., Zhang, Y., Medeiros, B., Pincus, R., . . . Ackerman, T. P.
641   (2012). Exposing Global Cloud Biases in the Community Atmosphere Model (CAM)
642   Using Satellite Observations and Their Corresponding Instrument Simulators. *Journal of*
643   *Climate, 25*(15), 5190-5207. 10.1175/jcli-d-11-00469.1
644 Klein, P. M., Hu, X. M., & Xue, M. (2014). Impacts of Mixing Processes in Nocturnal
645   Atmospheric Boundary Layer on Urban Ozone Concentrations. *Boundary-Layer*
646   *Meteorology, 150*(1), 107-130. 10.1007/s10546-013-9864-4

647   Langenbrunner, B., Pritchard, M. S., Kooperman, G. J., & Randerson, J. T. (2019). Why Does
648   Amazon Precipitation Decrease When Tropical Forests Respond to Increasing CO2?
649   *Earth's Future, 7*(4), 450-468. https://doi.org/10.1029/2018EF001026
650   Li, X. L., & Pu, Z. X. (2008). Sensitivity of Numerical Simulation of Early Rapid Intensification
651   of Hurricane Emily (2005) to Cloud Microphysical and Planetary Boundary Layer
652   Parameterizations. *Monthly Weather Review, 136*(12), 4819-4838.
653   10.1175/2008mwr2366.1
654   Lilly, D. K. (1968). Models of Cloud-Topped Mixed Layers under a Strong Inversion. *Quarterly*
655   *Journal of the Royal Meteorological Society, 94*(401), 292-&. DOI
656   10.1002/qj.49709440106
657   Liu, C., Ikeda, K., Rasmussen, R., Dominguez, F., Prein, A. F., Dudhia, J., & Chen, F. (2022).
658   *An Overview of Two-Decade-Long Convection Permitting Regional Climate*
659   *Downscaling over the Continental South America.* Paper presented at the AGU fall
660   meeting, Chicago, IL, https://agu.confex.com/agu/fm22/meetingapp.cgi/Paper/1115319.
661   Liu, M., & Carroll, J. J. (1996). A high-resolution air pollution model suitable for dispersion
662   studies in complex terrain. *Monthly Weather Review, 124*(10), 2396-2409. Doi
663   10.1175/1520-0493(1996)124<2396:Ahrapm>2.0.Co;2
664   Lu, X., & Wang, X. (2019). Improving Hurricane Analyses and Predictions with TCI, IFEX
665   Field Campaign Observations, and CIMSS AMVs Using the Advanced Hybrid Data
666   Assimilation System for HWRF. Part I: What is Missing to Capture the Rapid
667   Intensification of Hurricane Patricia (2015) when HWRF is already Initialized with a
668   More Realistic Analysis? *Monthly Weather Review, 147*(4), 1351-1373. 10.1175/mwr-d-
669   18-0202.1
670   Miguez-Macho, G., Stenchikov, G. L., & Robock, A. (2004). Spectral nudging to eliminate the
671   effects of domain position and geometry in regional climate model simulations. *Journal*
672   *of Geophysical Research-Atmospheres, 109*(D13). D13104, 10.1029/2003jd004495
673   Miguez-Macho, G., Stenchikov, G. L., & Robock, A. (2005). Regional climate simulations over
674   North America: Interaction of local processes with improved large-scale flow. *Journal of*
675   *Climate, 18*(8), 1227-1246. Doi 10.1175/Jcli3369.1
676   Nakanishi, M., & Niino, H. (2006). An Improved Mellor–Yamada Level-3 Model: Its Numerical
677   Stability and Application to a Regional Prediction of Advection Fog. *Boundary-Layer*
678   *Meteorology, 119*(2), 397-407. 10.1007/s10546-005-9030-8
679   Nielsen-Gammon, J. W., Hu, X.-M., Zhang, F., & Pleim, J. E. (2010). Evaluation of Planetary
680   Boundary Layer Scheme Sensitivities for the Purpose of Parameter Estimation. *Monthly*
681   *Weather Review, 138*(9), 3400-3417. 10.1175/2010mwr3292.1
682   Noh, Y., Cheon, W. G., Hong, S. Y., & Raasch, S. (2003). Improvement of the K-profile model
683   for the planetary boundary layer based on large eddy simulation data. *Boundary-Layer*
684   *Meteorology, 107*(2), 401-427. Doi 10.1023/A:1022146015946
685   Olson, J. B., Kenyon, J. S., Angevine, W. A., Brown, J. M., Pagowski, M., & Sušelj, K. (2019a).
686   A Description of the MYNN-EDMF Scheme and the Coupling to Other Components in
687   WRF–ARW. https://doi.org/10.25923/n9wm-be49
688   Olson, J. B., Kenyon, J. S., Djalalova, I., Bianco, L., Turner, D. D., Pichugina, Y., . . . Cline, J.
689   (2019b). Improving Wind Energy Forecasting through Numerical Weather Prediction
690   Model Development. *Bulletin of the American Meteorological Society, 100*(11), 2201-
691   2220. 10.1175/bams-d-18-0040.1

692   Painemal, D., Xu, K.-M., Cheng, A., Minnis, P., & Palikonda, R. (2015). Mean Structure and
693   Diurnal Cycle of Southeast Atlantic Boundary Layer Clouds: Insights from Satellite
694   Observations and Multiscale Modeling Framework Simulations. *Journal of Climate,*
695   *28*(1), 324-341. 10.1175/jcli-d-14-00368.1
696   Pergaud, J., Masson, V., Malardel, S., & Couvreux, F. (2009). A parameterization of dry
697   thermals and shallow cumuli for mesoscale numerical weather prediction. *Bound.-Layer*
698   *Meteor., 132*, 83-106.
699   Pleim, J. E. (2007). A combined local and nonlocal closure model for the atmospheric boundary
700   layer. Part I: Model description and testing. *Journal of Applied Meteorology and*
701   *Climatology, 46*(9), 1383-1395. 10.1175/Jam2539.1
702   Prein, A. F., Ge, M., Valle, A. R., Wang, D., & Giangrande, S. E. (2022). Towards a Unified
703   Setup to Simulate Mid-Latitude and Tropical Mesoscale Convective Systems at
704   Kilometer-Scales. *Earth and Space Science, 9*(8), e2022EA002295.
705   https://doi.org/10.1029/2022EA002295
706   Prein, A. F., Langhans, W., Fosser, G., Ferrone, A., Ban, N., Goergen, K., . . . Leung, R. (2015).
707   A review on regional convection-permitting climate modeling: Demonstrations,
708   prospects, and challenges. *Reviews of Geophysics, 53*(2), 323-361.
709   Prein, A. F., Rasmussen, R. M., Ikeda, K., Liu, C., Clark, M. P., & Holland, G. J. (2017). The
710   future intensification of hourly precipitation extremes. *Nature Clim. Change, 7*(1), 48-52.
711   10.1038/nclimate3168,
712   http://www.nature.com/nclimate/journal/v7/n1/abs/nclimate3168.html#supplementary-
713   information
714   Shin, H. H., & Hong, S. Y. (2011). Intercomparison of Planetary Boundary-Layer
715   Parametrizations in the WRF Model for a Single Day from CASES-99. *Boundary-Layer*
716   *Meteorology, 139*(2), 261-281. 10.1007/s10546-010-9583-z
717   Skamarock, W. C., & Klemp, J. B. (2008). A time-split nonhydrostatic atmospheric model for
718   weather research and forecasting applications. *Journal of Computational Physics, 227*(7),
719   3465-3485. http://dx.doi.org/10.1016/j.jcp.2007.01.037
720   Skamarock, W. C., Klemp, J. B., Dudhia, J., Gill, D. O., Liu, Z., Berner, J., . . . Huang, X.-y.
721   (2021). *A Description of the Advanced Research WRF Model Version 4.3*. (NCAR/TN-
722   556+STR). Retrieved from http://dx.doi.org/10.5065/1dfh-6p97.
723   Sun, X. G., Xue, M., Brotzge, J., McPherson, R. A., Hu, X. M., & Yang, X. Q. (2016). An
724   evaluation of dynamical downscaling of Central Plains summer precipitation using a
725   WRF-based regional climate model at a convection-permitting 4km resolution. *Journal of*
726   *Geophysical Research-Atmospheres, 121*(23), 13801-13825. 10.1002/2016jd024796
727   Supinie, T. A., Park, J., Snook, N., Hu, X. M., Brewster, K. A., Xue, M., & Carley, J. R. (2022).
728   Cool-Season Evaluation of FV3-LAM-Based CONUS-Scale Forecasts with Physics
729   Configurations of Experimental RRFS Ensembles. *Monthly Weather Review, 150*(9),
730   2379-2398. 10.1175/mwr-d-21-0331.1
731   Tai, S.-L., Feng, Z., Ma, P.-L., Schumacher, C., & Fast, J. D. (2021). Representations of
732   Precipitation Diurnal Cycle in the Amazon as Simulated by Observationally Constrained
733   Cloud-System Resolving and Global Climate Models. *Journal of Advances in Modeling*
734   *Earth Systems, 13*(11), e2021MS002586. https://doi.org/10.1029/2021MS002586
735   Thompson, G., Field, P. R., Rasmussen, R. M., & Hall, W. D. (2008). Explicit Forecasts of
736   Winter Precipitation Using an Improved Bulk Microphysics Scheme. Part II:

737   Implementation of a New Snow Parameterization. *Monthly Weather Review, 136*(12),
738   5095-5115. 10.1175/2008mwr2387.1
739 Tiedtke, M. (1989). A Comprehensive Mass Flux Scheme for Cumulus Parameterization in
740   Large-Scale Models. *Monthly Weather Review, 117*(8), 1779-1800. Doi 10.1175/1520-
741   0493(1989)117<1779:Acmfsf>2.0.Co;2
742 Troen, I., & Mahrt, L. (1986). A Simple-Model of the Atmospheric Boundary-Layer - Sensitivity
743   to Surface Evaporation. *Boundary-Layer Meteorology, 37*(1-2), 129-148. Doi
744   10.1007/Bf00122760
745 Vera, C., Silvestri, G., Liebmann, B., & González, P. (2006). Climate change scenarios for
746   seasonal precipitation in South America from IPCC-AR4 models. *Geophysical Research
747   Letters, 33*(13). https://doi.org/10.1029/2006GL025759
748 Wang, J. L., & Kotamarthi, V. R. (2013). Assessment of Dynamical Downscaling in Near-
749   Surface Fields with Different Spectral Nudging Approaches Using the Nested Regional
750   Climate Model (NRCM). *Journal of Applied Meteorology and Climatology, 52*(7), 1576-
751   1591. 10.1175/Jamc-D-12-0302.1
752 Wang, J. X., & Hu, X. M. (2021). Evaluating the Performance of WRF Urban Schemes and PBL
753   Schemes over Dallas-Fort Worth during a Dry Summer and a Wet Summer. *Journal of
754   Applied Meteorology and Climatology, 60*(6), 779-798. 10.1175/Jamc-D-19-0195.1
755 Wang, W. G., Shen, X. Y., & Huang, W. Y. (2016). A Comparison of Boundary-Layer
756   Characteristics Simulated Using Different Parametrization Schemes. *Boundary-Layer
757   Meteorology, 161*(2), 375-403. 10.1007/s10546-016-0175-4
758 Wright, J. S., Fu, R., Worden, J. R., Chakraborty, S., Clinton, N. E., Risi, C., . . . Yin, L. (2017).
759   Rainforest-initiated wet season onset over the southern Amazon. *Proceedings of the
760   National Academy of Sciences, 114*(32), 8481-8486. doi:10.1073/pnas.1621516114
761 Wu, M., Lee, J.-E., Wang, D., & Salameh, M. (2021a). Suppressed Daytime Convection Over
762   the Amazon River. *Journal of Geophysical Research: Atmospheres, 126*(13),
763   e2020JD033627. https://doi.org/10.1029/2020JD033627
764 Wu, Z., Li, Y., Li, X., Hu, X.-M., Zhou, G., & Deng, C. (2021b). Influence of Different
765   Planetary Boundary Layer Parameterization Schemes on the Simulation of Precipitation
766   Caused by Southwest China Vortex in Sichuan Basin Based on the WRF Model. *Chinese
767   Journal of Atmospheric Sciences, 45*(1), 58. 10.3878/j.issn.1006-9895.2005.19171
768 Xie, B., Fung, J. C. H., Chan, A., & Lau, A. (2012). Evaluation of nonlocal and local planetary
769   boundary layer schemes in the WRF model. *Journal of Geophysical Research:
770   Atmospheres, 117*(D12). https://doi.org/10.1029/2011JD017080
771 Yang, Y., Hu, X.-M., Gao, S., & Wang, Y. (2019). Sensitivity of WRF simulations with the YSU
772   PBL scheme to the lowest model level height for a sea fog event over the Yellow Sea.
773   *Atmospheric Research, 215*, 253-267. https://doi.org/10.1016/j.atmosres.2018.09.004
774 Zhang, D., Wang, Z., & Liu, D. (2010). A global view of midlevel liquid-layer topped stratiform
775   cloud distribution and phase partition from CALIPSO and CloudSat measurements.
776   *Journal of Geophysical Research: Atmospheres, 115*(D4).
777   https://doi.org/10.1029/2009JD012143
778 Zhang, Y., Jiang, Y., & Tan, B. (2013). Influences of different PBL schemes on secondary
779   eyewall formation and eyewall replacement cycle in simulated Typhoon Sinlaku (2008).
780   *Acta Meteorologica Sinica, 27*, 322-334. 10.1007/s13351-013-0312-7
781 Zhu, P., Hazelton, A., Zhang, Z., Marks, F. D., & Tallapragada, V. (2021). The Role of Eyewall
782   Turbulent Transport in the Pathway to Intensification of Tropical Cyclones. *Journal of

783   *Geophysical Research: Atmospheres, 126*(17), e2021JD034983.
784   https://doi.org/10.1029/2021JD034983
785 Zhu, P., Tyner, B., Zhang, J. A., Aligo, E., Gopalakrishnan, S., Marks, F. D., . . . Tallapragada,
786   V. (2019). Role of eyewall and rainband eddy forcing in tropical cyclone intensification.
787   *Atmos. Chem. Phys., 19*(22), 14289-14310. 10.5194/acp-19-14289-2019
788
789

790 Table 1. Model configuration for sensitivity simulations modifying parameters and treatments in
791 the YSU and ACM2 PBL schemes. *p* is an exponent in the polynomial function determining
792 vertical mixing strength in the PBL, λ is the asymptotic length scale.

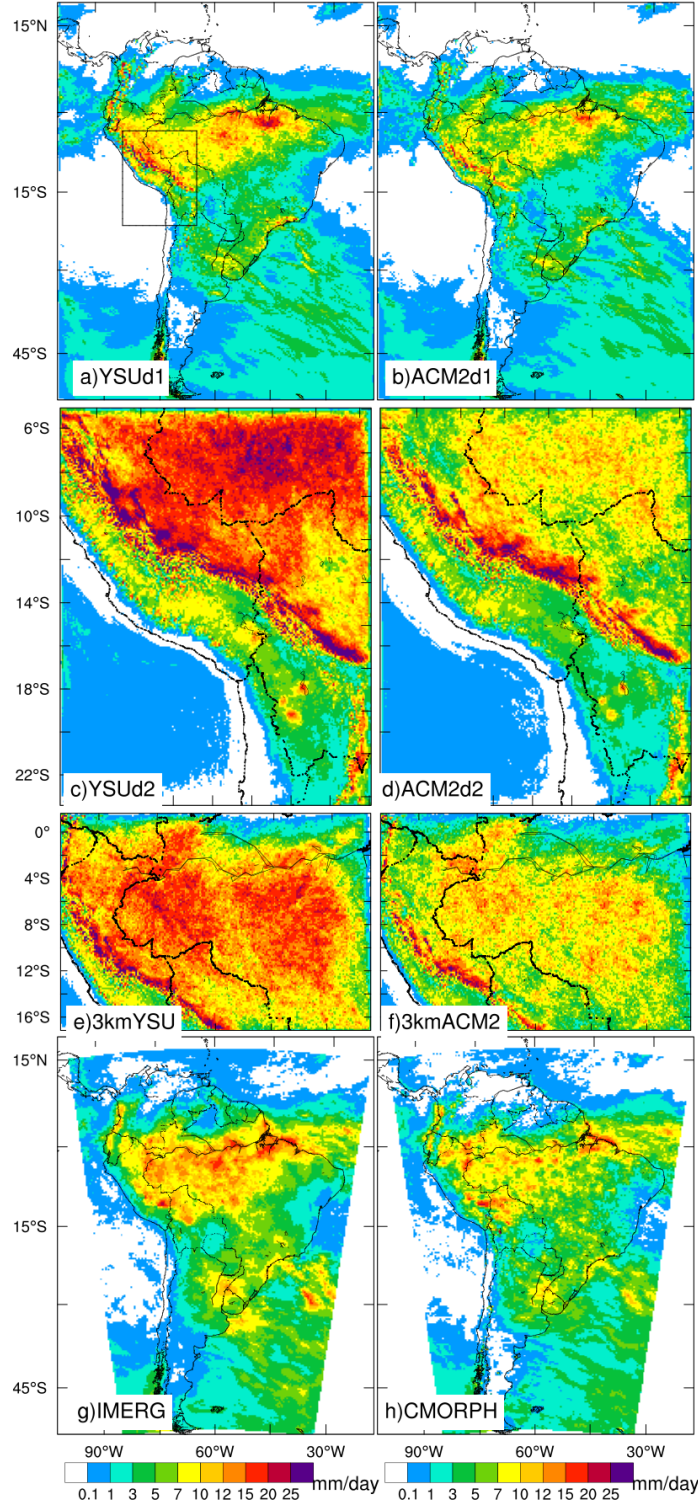| PBL	Grid spacings	Experiment name	Changed parameters/treatments
YSU	15 km	YSU	*p=2* (default)
		YSUp.5	*p=0.5*
		YSUuseACM2free	Use free troposphere treatment from ACM2
		YSUp.5useACM2free	*p=0.5 &* use free troposphere treatment from ACM2
	3km	3kmYSU	*p=2* (default)
		3kmYSUp.5	*p=0.5*
		3kmYSUp.5useACM2free	*p=0.5 &* use free troposphere treatment from ACM2
ACM2	15 km	ACM2	$\lambda=80$ (default)
		ACM2λ30	$\lambda=30$
	3 km	3kmACM2	$\lambda=80$ (default)

793

794

795 **Figures**
796 Figure 1. Daily mean precipitation rate in Jan-Feb 2019 simulated with (a) YSU in domain 1, (b)
797 ACM2 in domain 1 with a 15 km grid spacing, (c) YSU in domain 2, (d) ACM2 in domain 2 with
798 a 3 km grid spacing, (e) single-domain YSU, (f) single-domain ACM2 with a 3 km grid spacing
799 and from (g) IMERG, (h) CMORPH data. The rectangle in (a) marks the location of the nested
800 domain.
801

802 Figure 2. Hourly mean precipitation rate at 18 UTC (14 LST) in Jan-Feb 2019 simulated with (a)
803 YSU in domain 1, (b) ACM2 in domain 1, (c) YSU in domain 2, (d) ACM2 in domain 2, (e) single-
804 domain YSU, (f) single-domain ACM2 and observed from (g) IMERG, (h) CMORPH.
805

806 Figure 3. Average surface temperature at 17 UTC in Jan-Feb 2019 from (a,c,e) YSU, (b,d,f) ACM2,
807 and (g,h,i) their difference (ACM2-YSU) in (top to bottom) different domains. The average
808 difference over land is marked at the lower-left corner in (g,h,i)
809

810 Figure 4. Average surface downward shortwave radiation at 17 UTC in Jan-Feb 2019 simulated
811 with (a,c,e) YSU, (b,d,f) ACM2, (g,h,i) their difference, and (j,k,l) column-average cloud water
812 mixing ratios in (top to bottom) different domains. The straight dash lines mark the location of
813 cross-sections in Figs. 5, 6, and 11.
814

815 Figure 5. Cross-section of cloud water over the Amazon in Jan-Feb 2019 simulated by (left) YSU
816 and (right) ACM2 at (a,b) 11, (c,d) 14, (e,f) 17, and (g,h) 21 UTC (7, 10, 13, 17 LST
817 correspondingly). The location of these cross-sections is marked in Fig. 4j
818

819   Figure 6. Cross-section of cloud water over the Amazon in Jan-Feb 2019 simulated by (a) YSU
820   and (b) ACM2, (c) $YSUp.5$, (d) $YSUuseACM2free$, (e) $YSUp.5useACM2free$, (f) ACM2λ30 at 17
821   UTC. The location of these cross-sections is marked in Fig. 4j

823   Figure 7. Average surface downward shortwave radiation at 17 UTC during January-February
824   2019 simulated by (a) YSU, (b) ACM2 and 4 sensitivity simulations (c) $YSUp.5$, (d)
825   $YSUuseACM2free$, (e) $YSUp.5useACM2free$, (f) ACM2λ30.

827   Figure 8. Average CAPE at 17 UTC during January-February 2019 simulated by (a) YSU, (b)
828   ACM2 and 4 sensitivity simulations (c) $YSUp.5$, (d) $YSUuseACM2free$, (e) $YSUp.5useACM2free$,
829   (f) ACM2λ30.

831   Figure 9. Mean profiles of (a) water vapor mixing ratio, (b) water vapor difference from that
832   simulated by YSU, (c) cloud water mixing ratio (QCLOUD), and (d) vertical mixing coefficient
833   (K_z) at 17 UTC during January-February 2019 at Manaus (location marked in Fig. 8b) simulated
834   by YSU, ACM2 and 4 sensitivity simulations $YSUp.5, YSUuseACM2free, YSUp.5useACM2free$,
835   ACM2λ30.

837   Figure 10. Average precipitation rate at 18 UTC during January-February 2019 simulated by (a)
838   YSU, (b) ACM2 and 4 sensitivity simulations (c) $YSUp.5$, (d) $YSUuseACM2free$, (e)
839   $YSUp.5useACM2free$, (f) ACM2λ30.

841   Figure 11. Cross-section of average noon-time cloud water mixing ratios over the Amazon in Jan-
842   Feb 2019 simulated by (a) $3kmYSU$, (b) $3kmACM2$, (c) $3kmYSUp.5$, and (d)
843   $3kmYSUp.5useACM2free$. The location of these cross-sections is marked in Fig. 4l

845   Figure 12. Average noon-time precipitation rate in Jan-Feb 2019 simulated by (a) $3kmYSU$, (b)
846   $3kmACM2$, (c) $3kmYSUp.5$, and (d) $3kmYSUp.5useACM2free$. The domain-averaged values are
847   marked.
848

Figure 1. Daily mean precipitation rate in Jan-Feb 2019 simulated with (a) YSU in domain 1, (b) ACM2 in domain 1 with a 15 km grid spacing, (c) YSU in domain 2, (d) ACM2 in domain 2 with a 3 km grid spacing, (e) single-domain YSU, (f) single-domain ACM2 with a 3 km grid spacing and from (g) IMERG, (h) CMORPH data. The rectangle in (a) marks the location of the nested domain.
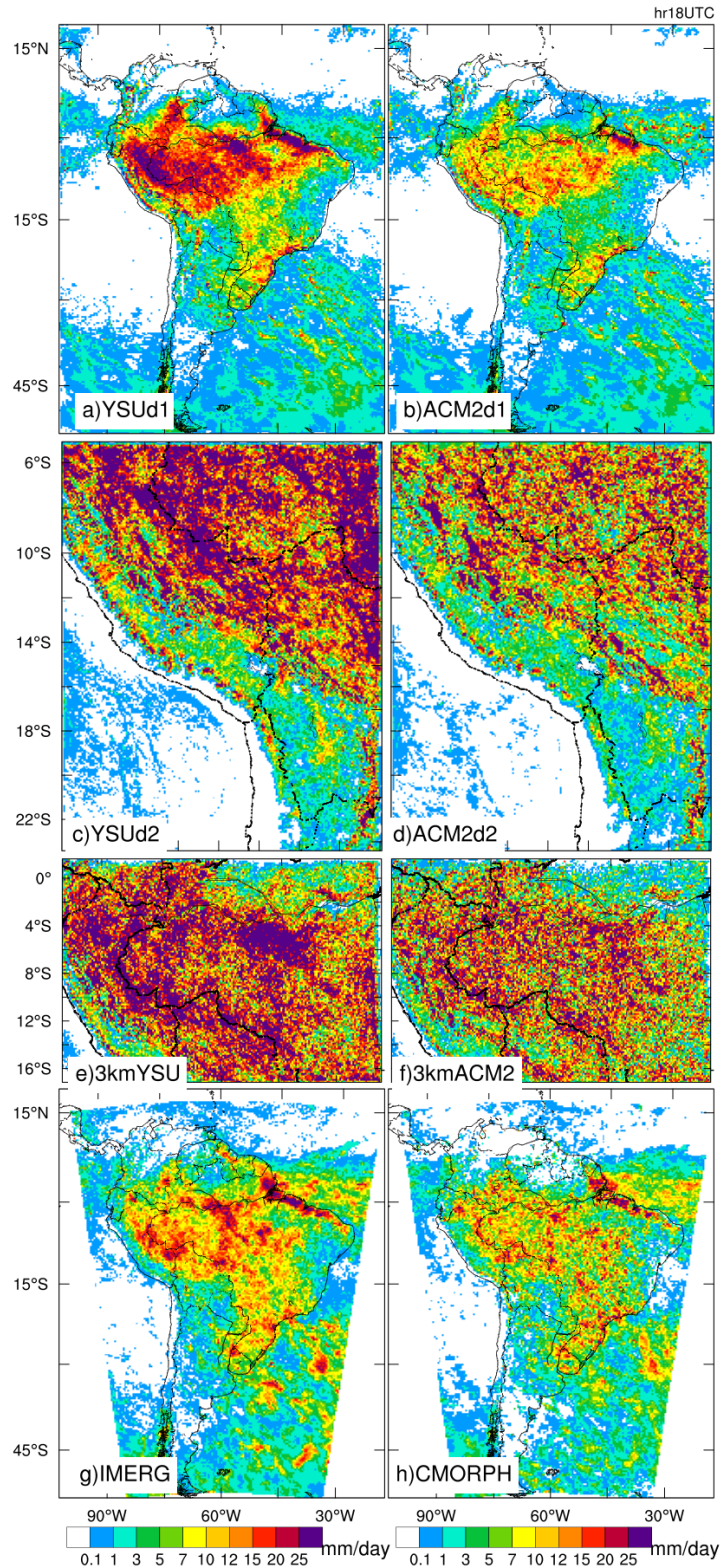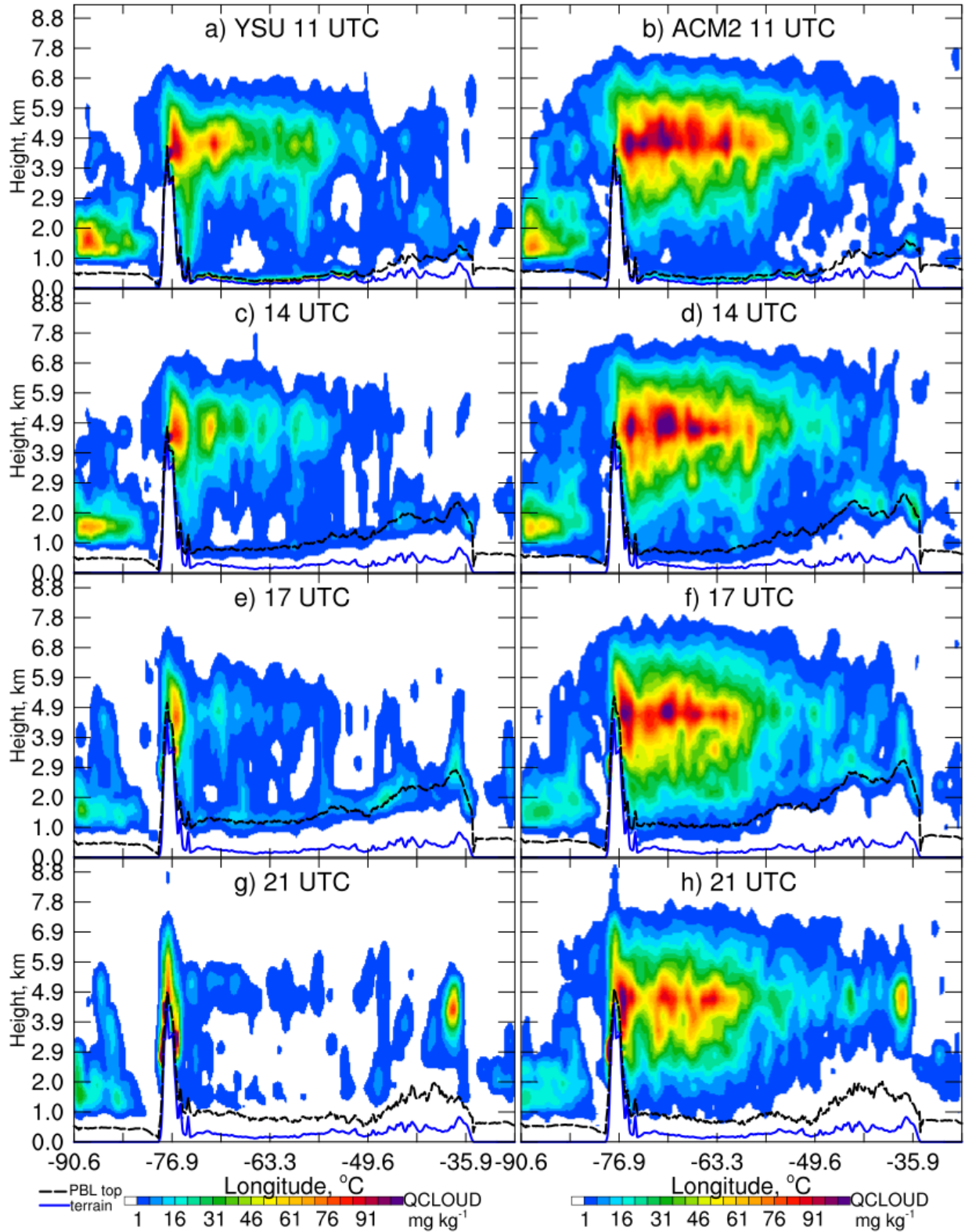
Figure 2. Hourly mean precipitation rate at 18 UTC (14 LST) in Jan-Feb 2019 simulated with (a) YSU in domain 1, (b) ACM2 in domain 1, (c) YSU in domain 2, (d) ACM2 in domain 2, (e) single-domain YSU, (f) single-domain ACM2 and observed from (g) IMERG, (h) CMORPH.

Figure 3. Average surface temperature at 17 UTC in Jan-Feb 2019 from (a,c,e) YSU, (b,d,f) ACM2, and (g,h,i) their difference (ACM2-YSU) in (top to bottom) different domains. The average difference over land is marked at the lower-left corner in (g,h,i)

Figure 4. Average surface downward shortwave radiation at 17 UTC in Jan-Feb 2019 simulated with (a,c,e) YSU, (b,d,f) ACM2, (g,h,i) their difference, and (j,k,l) column-average cloud water mixing ratios in (top to bottom) different domains. The straight dash lines mark the location of cross-sections in Figs. 5, 6, and 11.

Figure 5. Cross-section of cloud water over the Amazon in Jan-Feb 2019 simulated by (left) YSU and (right) ACM2 at (a,b) 11, (c,d) 14, (e,f) 17, and (g,h) 21 UTC (7, 10, 13, 17 LST correspondingly). The location of these cross-sections is marked in Fig. 4j

Figure 6. Cross-section of cloud water over the Amazon in Jan-Feb 2019 simulated by (a) YSU and (b) ACM2, (c) YSUp.5, (d) YSUuseACM2free, (e) YSUp.5useACM2free, (f) ACM2λ30 at 17 UTC. The location of these cross-sections is marked in Fig. 4j

Figure 7. Average surface downward shortwave radiation at 17 UTC during January-February 2019 simulated by (a) YSU, (b) ACM2 and 4 sensitivity simulations (c) YSUp.5, (d) YSUuseACM2free, (e) YSUp.5useACM2free, (f) ACM2λ30.
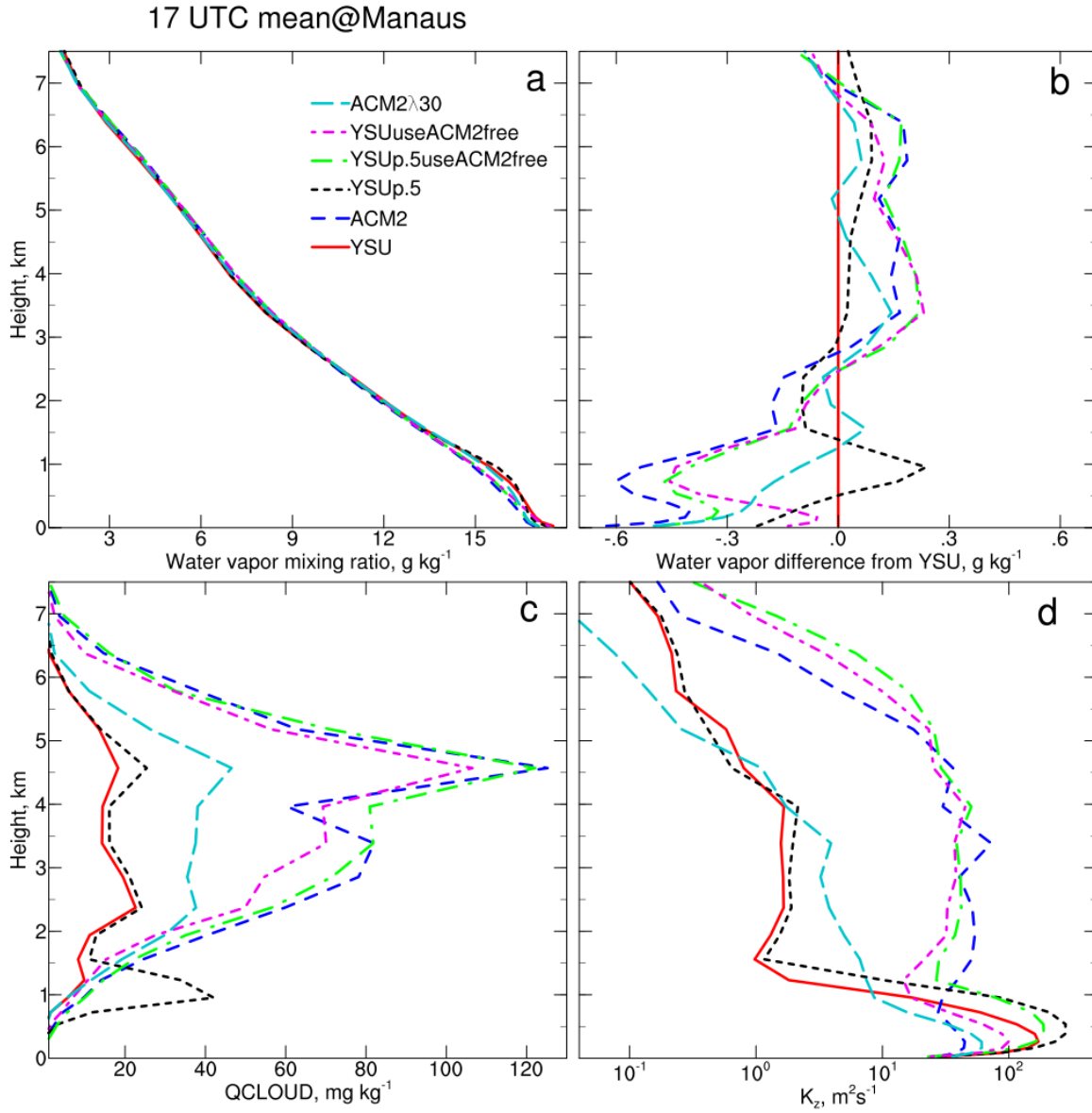
Figure 8. Average CAPE at 17 UTC during January-February 2019 simulated by (a) YSU, (b) ACM2 and 4 sensitivity simulations (c) YSUp. 5, (d) YSUuseACM2free, (e) YSUp. 5useACM2free, (f) ACM2λ30.

Figure 9. Mean profiles of (a) water vapor mixing ratio, (b) water vapor difference from that simulated by YSU, (c) cloud water mixing ratio (QCLOUD), and (d) vertical mixing coefficient (K_z) at 17 UTC during January-February 2019 at Manaus (location marked in Fig. 8b) simulated by YSU, ACM2 and 4 sensitivity simulations YSUp.5, YSUuseACM2free, YSUp.5useACM2free, ACM2λ30.
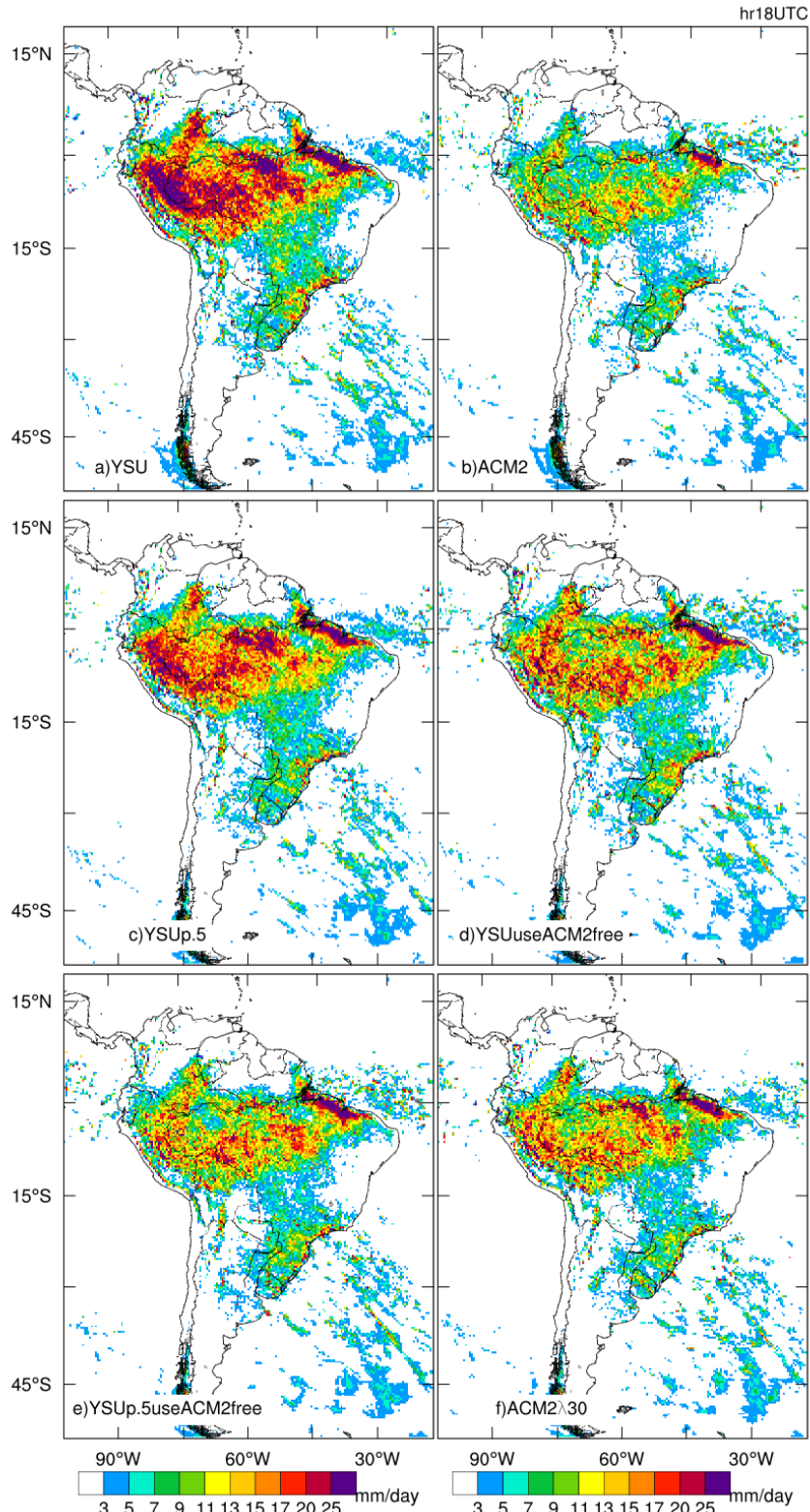
Figure 10. Average precipitation rate at 18 UTC during January-February 2019 simulated by (a) YSU, (b) ACM2 and 4 sensitivity simulations (c) YSUp.5 , (d) YSUuseACM2free , (e) YSUp.5useACM2free, (f) ACM2λ30.
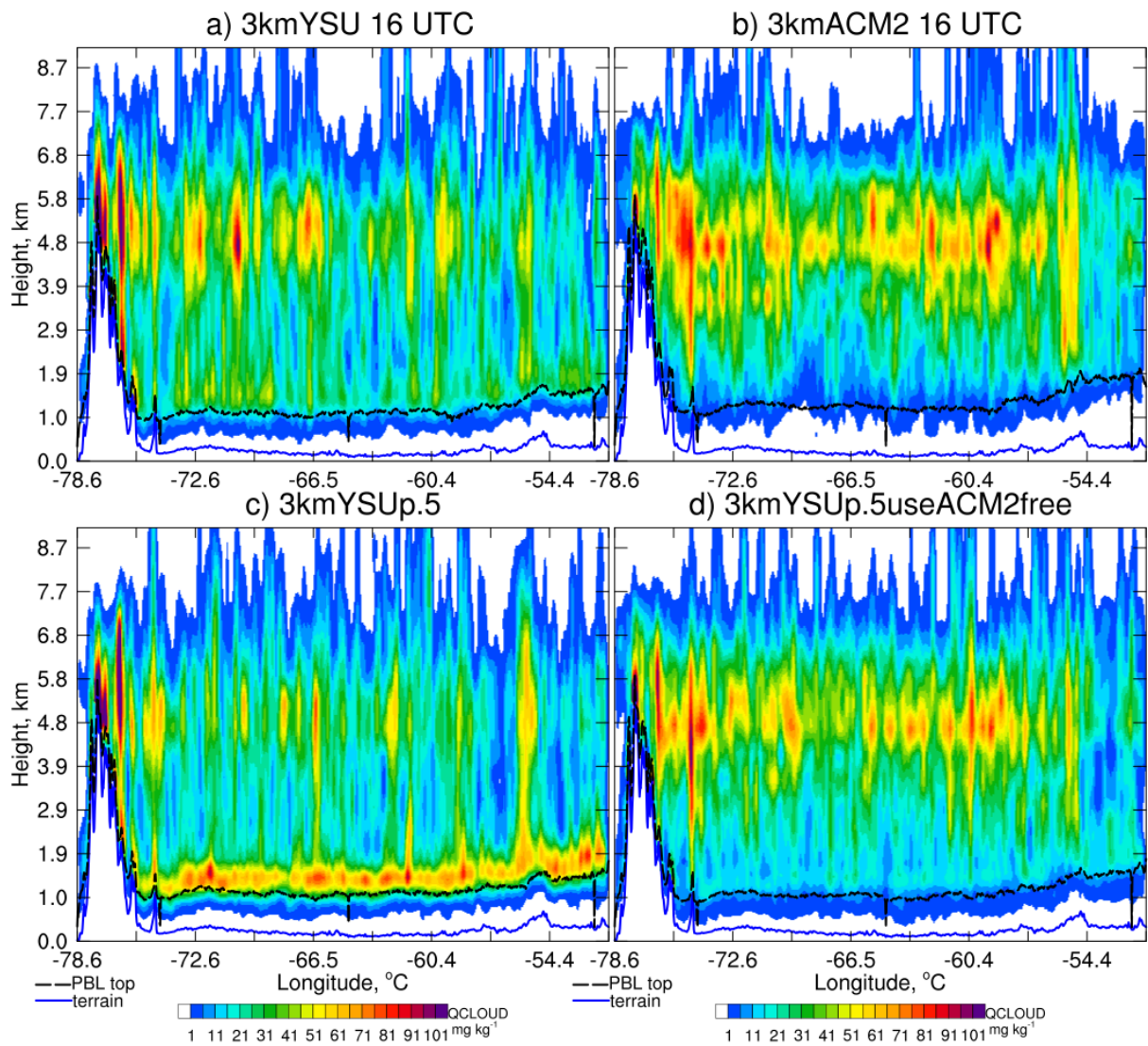
Figure 11. Cross-section of average noon-time cloud water mixing ratios over the Amazon in Jan-Feb 2019 simulated by (a) 3kmYSU , (b) 3kmACM2 , (c) 3kmYSUp. 5 , and (d) 3kmYSUp. 5useACM2free. The location of these cross-sections is marked in Fig. 4l
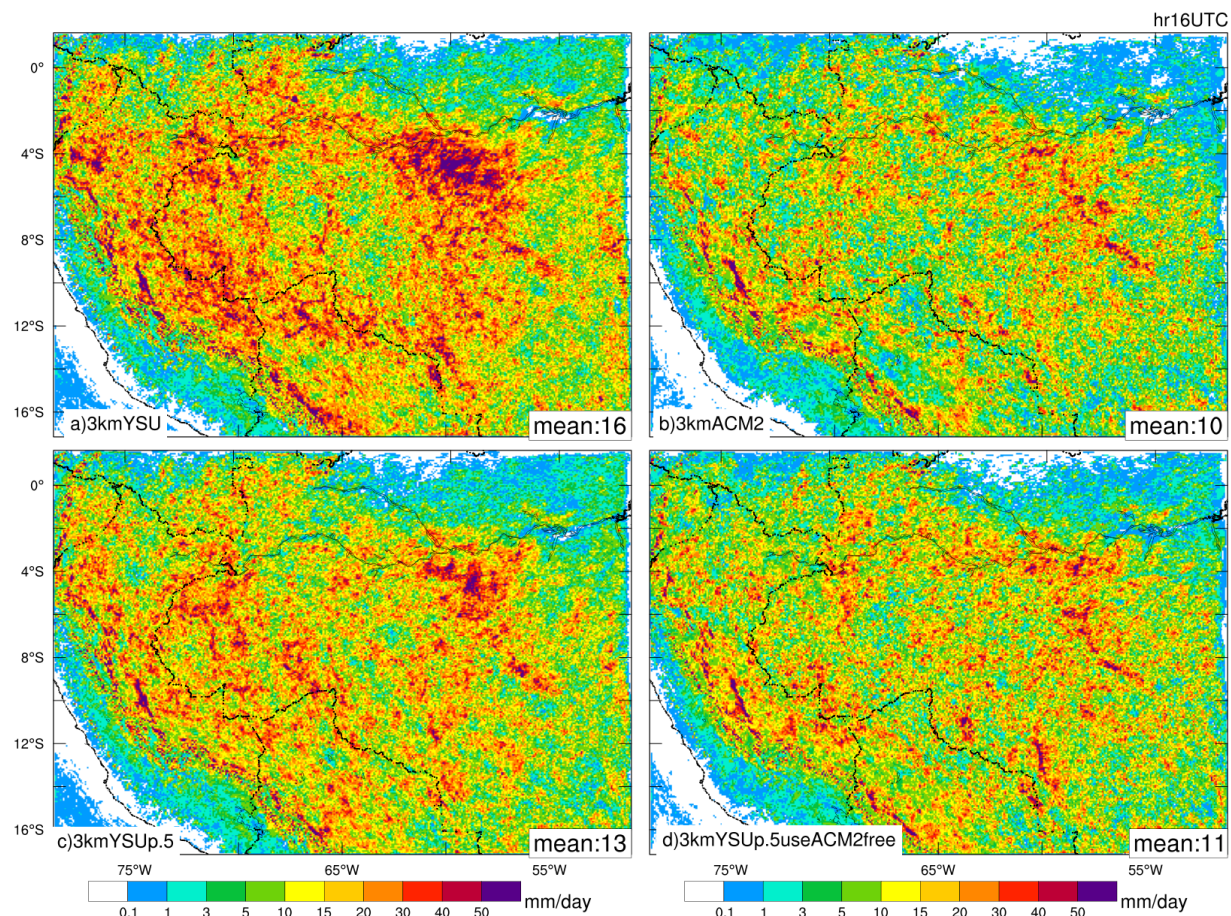
Figure 12. Average noon-time precipitation rate in Jan-Feb 2019 simulated by (a) 3kmYSU, (b) 3kmACM2, (c) 3kmYSUp.5, and (d) 3kmYSUp.5useACM2free. The domain-averaged values are marked.